Cerebral Cortex, September 2018;28: 3278–3294

doi: 10.1093/cercor/bhx199
Advance Access Publication Date: 1 August 2017
Original Article

ORIGINAL ARTICLE

Transcription Factors *Sp8* and *Sp9* Coordinately Regulate Olfactory Bulb Interneuron Development

Jiwen Li[1], Chunyang Wang[1], Zhuangzhi Zhang[1], Yan Wen[1], Lei An[1], Qifei Liang[1], Zhejun Xu[1], Song Wei[1], Weiwei Li[1], Teng Guo[1], Guoping Liu[1], Guangxu Tao[1], Yan You[1], Heng Du[1], Zhuoning Fu[1], Miao He[1], Bin Chen[2], Kenneth Campbell[3], Arturo Alvarez-Buylla[4], John L. Rubenstein[5] and Zhengang Yang[1]

[1]Department of Translational Neuroscience, Shanghai Pudong Hospital, State Key Laboratory of Medical Neurobiology, Institutes of Brain Science, and Collaborative Innovation Center for Brain Science, Fudan University, Shanghai 200032, China, [2]Department of Molecular, Cell and Developmental Biology, University of California, Santa Cruz, CA 95064, USA, [3]Division of Developmental Biology, Cincinnati Children's Hospital Medical Center, University of Cincinnati College of Medicine, Cincinnati, OH 45229, USA, [4]Department of Neurological Surgery, The Eli and Edythe Broad Center of Regeneration Medicine and Stem Cell Research, University of California, San Francisco, CA 94143, USA and [5]Department of Psychiatry, Nina Ireland Laboratory of Developmental Neurobiology, UCSF Weill Institute for Neurosciences, University of California, San Francisco, CA 94158, USA

Address correspondence to Zhengang Yang, State Key Laboratory of Medical Neurobiology and Institutes of Brain Science, Fudan University, 138 Yi Xue Yuan Road, Shanghai 200032, China. Email: yangz@fudan.edu.cn

Jiwen Li and Chunyang Wang contributed equally to this work

Abstract

Neural stem cells in the postnatal telencephalic ventricular-subventricular zone (V-SVZ) generate new interneurons, which migrate tangentially through the rostral migratory stream (RMS) into the olfactory bulb (OB). The Sp8 and Sp9 transcription factors are expressed in neuroblasts, as well as in the immature and mature interneurons in the V-SVZ–RMS–OB system. Here we show that *Sp8* and *Sp9* coordinately regulate OB interneuron development: although *Sp9* null mutants show no major OB interneuron defect, conditional deletion of both *Sp8* and *Sp9* resulted in a much more severe reduction of OB interneuron number than that observed in the *Sp8* conditional mutant mice, due to defects in neuronal differentiation, tangential and radial migration, and increased cell death in the V-SVZ–RMS–OB system. RNA-Seq and RNA in situ hybridization reveal that, in *Sp8/Sp9* double mutant mice, but not in *Sp8* or *Sp9* single mutant mice, newly born neuroblasts in the V-SVZ–RMS–OB system fail to express *Prokr2* and *Tshz1* expression, genes with known roles in promoting OB interneuron differentiation and migration, and that are involved in human Kallmann syndrome.

Key words: interneuron, Kallmann syndrome, migration, olfactory bulb, *Prokr2*, *Sp8*, *Sp9*, *Tshz1*

Introduction

The mammalian olfactory bulb (OB) is composed of 2 main types of neurons: projection neurons and interneurons. While transmission of olfactory information to the pyriform and entorhinal cortex is mediated by the glutamatergic projection neurons (mitral/tufted cells), the vast majority of neurons in the OB are the GABAergic interneurons, including the granular, external plexiform and periglomerular subtypes (Shepherd et al. 2007; Nagayama et al. 2014; Lim and Alvarez-Buylla 2016). During embryonic development (~E12–E14), OB interneurons begin to be generated from neural stem/progenitor cells located primarily in the dorsal lateral ganglionic eminence (dLGE) and along the rostral migratory stream (RMS) (Wichterle et al. 2001; Stenman et al. 2003; Tucker et al. 2006; Long et al. 2007). OB interneurons continue to be generated in the postnatal and adult brain. Neural stem cells in the ventricular-subventricular zone (V-SVZ) in different regions of the V-SVZ, facing the cortex, striatum and septum, as well as in the RMS, produce different types of OB interneurons (Vergano-Vera et al. 2006; Kohwi et al. 2007; Merkle et al. 2007, 2014; Young et al. 2007; Alonso et al. 2008; Bartolini et al. 2013).

The process of OB interneuron generation in the adult brain includes several steps: (1) their initial genesis from GFAP-expressing astroglial primary neural stem cells (known as B1 cells); (2) the amplification of the lineage through the generation of intermediate neural progenitors (C cells) (Doetsch et al. 1999, 2002; Mirzadeh et al. 2008); (3) the initial differentiation as C cells give rise to the migrating neuroblasts (A cells) (Doetsch et al. 1997; Ponti et al. 2013); (4) tangential migration of neuroblasts aligning into chains along the V-SVZ and RMS into the core of the OB (the end of the RMS) (Lois and Alvarez-Buylla 1994; Lois et al. 1996); (5) radial migration of the young neurons as individual cells from the core of the OB into specific layers; and (6) final maturation and differentiation into functional interneurons (Hack et al. 2002; Carleton et al. 2003; Saghatelyan et al. 2004). These processes are normally then followed by a wave of programmed cell death that occurs after the new neurons have fully formed dendrites and synaptic spines (Petreanu and Alvarez-Buylla 2002).

The transcription factor *Sp8*, initially expressed in the embryonic dLGE, continues to be expressed in the postnatal and adult V-SVZ–RMS–OB. Its expression persists from the dividing neuroblasts to the vast majority of mature interneurons. (Waclaw et al. 2006; Liu et al. 2009; Wei et al. 2011; Kosaka and Kosaka 2012). *Dlx5/6-Cre-IRES-EGFP* (*Dlx5/6-CIE*) transgenic mice express both Cre recombinase and GFP under the control of the *Dlx5/6* enhancer element id6/id5 in nearly all telencephalic GABAergic neurons (Zerucha et al. 2000; Stenman et al. 2003). In *Dlx5/6-CIE; Sp8*$^{F/F}$ mice (referred to herein as *Sp8-CKO* mice), a large number of glutamate decarboxylase 1-expressing (GAD1$^+$) and calbindin 2 (calretinin)-expressing (CR$^+$) interneurons in the OB granule cell layer (GCL) and glomerular layer, and about 80% parvalbumin expressing (PV$^+$) interneurons in the OB external plexiform layer (EPL) are lost (Waclaw et al. 2006; Li et al. 2011).

Recently, we have showed that *Sp9*, a *Sp* family member which closely resembles *Sp8* (Kawakami et al. 2004; Zhao and Meng 2005), is widely expressed in the embryonic ganglionic eminences and that Sp9$^+$ cells give rise to the majority of OB interneurons (Zhang et al. 2016). Given the high homology of *Sp8* and *Sp9*, we asked whether *Sp9* regulates OB interneuron development, especially in the context of a possible interplay with *Sp8*.

Here, we show that, like *Sp8*, *Sp9* is also expressed in the adult V-SVZ–RMS–OB system. Most Sp9$^+$ cells are neuroblasts, but a few correspond to intermediate progenitors. Although germline knockout of *Sp9 (Sp9-KO)* did not lead to obvious defects in OB interneurons, conditional ablation of both *Sp8* and *Sp9* with *Dlx5/6-CIE* (*Sp8/Sp9-DCKO*) led to a much enhanced loss of OB interneurons than that observed in the *Sp8-CKO* mice. Close inspection of the development of OB interneurons in the double mutants revealed blockage of neuronal differentiation in embryonic and postnatal neural progenitors, defect in tangential and radial migration of neuroblasts, and increased cell death in the V-SVZ–RMS–OB system. RNA sequencing (RNA-Seq) and in situ hybridization showed that Sp8 and Sp9 coordinately induce *prokineticin receptor 2 (Prokr2)* and transcription factor *teashirt zinc finger family member 1 (Tshz1)* expression, genes essential for OB interneuron differentiation, migration and survival. These 2 genes are also known to involved in human Kallmann syndrome, which is characterized by congenital hypogonadotropic hypogonadism (due to gonadotropin-releasing hormone [GnRH] deficiency) and anosmia/hyposmia (due to defects in OB development) (Ng et al. 2005; Dode et al. 2006; Matsumoto et al. 2006; Pitteloud et al. 2007; Prosser et al. 2007; Sarfati et al. 2010; Martin et al. 2011; Ragancokova et al. 2014). Thus, our results demonstrate that *Sp8* and *Sp9* have crucial roles in regulating OB interneuron development.

Materials and Methods

Mice

Sp9$^{LacZ/+}$ (Zhang et al. 2016), *Sp9* floxed (Zhang et al. 2016), *Sp8* floxed (Bell et al. 2003), *hGFAP-Cre* (Zhuo et al. 2001), *Dlx5/6-CIE* (Stenman et al. 2003), and *Rosa-YFP* (Srinivas et al. 2001) mice were previously described. These mice were maintained in a mixed genetic background of C57BL/6J, 129S6, and CD1. The day of vaginal plug detection was calculated as embryonic day 0.5, and the day of birth was considered as postnatal day 0. All animal experiments described in this study were approved in accordance with institutional guidelines.

Tissue Preparation

Postnatal mice were deeply anesthetized and perfused intracardially with 4% PFA in 1× phosphate buffered saline (PBS, pH 7.4); embryonic brains were immersion fixed in 4% PFA. All brains were fixed overnight in 4% PFA, cryoprotected in 30% sucrose for at least 24 h, frozen in the embedding medium and cryosectioned.

BrdU Labeling

Single intraperitoneal injections of BrdU (100 mg/kg) were given to control and *hGFAP-Cre*; *Sp8*$^{F/F}$; *Sp9*$^{F/F}$ mice at P60. Mice were sacrificed 1 h after BrdU injection.

Viral Infection

P0 mouse pups were deeply anesthetized on ice. 0.05 μl Ad-Cre (1×10^{10} cfu/ml) was injected to the dorsolateral V-SVZ (Merkle et al. 2007) using a microinjector on a stereotaxic injection station. After injection, pups were returned to their mother. Mice were sacrificed at P7 and P21.

Histochemistry

Procedures for 5-bromo-4-chloro-3-indoyl-D-galactopyranoside (X-gal) staining was performed as described previously (Wang et al. 2011). Briefly, $Sp9^{Lacz/+}$ mice were perfused with 4% PFA. The 30 μm sections were washed twice (5 min each) in X-gal wash (0.1 M sodium phosphate buffer, pH 7.4, 2 mM $MgCl_2$, 5 mM EGTA, 0.01% sodium deoxycholate, 0.02% Nonidet P-40) and stained at 37°C for 1–5 h in X-gal staining solution (X-gal wash plus 5 mM potassium ferricyanide, 5 mM potassium ferrocyanide, 1 mg/ml X-gal).

Immunohistochemistry

Immunohistochemistry was performed on 12 μm cryostat sections on slides, or 30–50 μm free floating sections (Ma et al. 2013; Zhang et al. 2016). For Sp9 immunohistochemistry, sections were boiled in 10 mM sodium citrate briefly for antigen retrieval. BrdU labeled sections were incubated in 2 N HCl for 1 h at room temperature, and then rinsed in 0.1 M borate buffer twice. The following primary antibodies were used: goat anti-Sp8 (1:1000, Santa Cruz, sc-104 661), rabbit anti-Sp9 (1:500) (Zhang et al. 2016), rabbit anti-CR (1:2000, Swant, 7699/3H), mouse anti-CR (1:1000, Swant, 6B3), rabbit anti-PV (1:3000, Swant,PV25), mouse anti-PV (1/1000, Sigma, P3088), rabbit anti-CB (1:10 000, Swant,CB38), mouse anti-CB (1:10 000, Swant, 300), mouse anti-TH (tyrosine hydroxylase, 1:400, Millipore, MAB318), chicken anti-GFP (1:3000, Aves Labs, GFP-1020), goat anti-DCX (1:1000, Santa Cruz, sc-8066), mouse anti-PSA-NCAM (1:1000, Millipore, MAB5324), mouse anti-NeuN (1:500, Millipore, MAB-377), rat anti-BrdU (1:50, Accurate Chemical, OBT0030s), rabbit anti-Ascl1 (1:2000, Cosmo Bio, SK-T01-003), rabbit anti-Gsx2 (1:2000, Millipore, ABN162), and rabbit anti-cleaved Caspase-3 (1:500, Cell Signaling, 9661L).

In Situ RNA Hybridization

All in situ RNA hybridization experiments were performed using digoxigenin riboprobes on 20 μm cryostat sections (Long et al. 2009; Zhang et al. 2016). Riboprobes were made from cDNAs amplified by PCR using the following primers:

Gad1 Forward: ATGGCATCTTCCACTCCTTCG
Gad1 Reverse: TTACAGATCCTGACCCAACCTCTC
Tshz1 Forward: GAGAAGGTCACGGGCAAGGTCAGC
Tshz1 Reverse: GAGGCGAGGACACAGCATCTGCCA
Prokr2 Forward: ATGGGACCCCAGAACAGA
Prokr2 Reverse: ATGGGACCCCAGAACAGA
Reln Forward: CACCTACTACGTACCGGGACAGGA
Reln Reverse: AGGCTGTCCTGTTTCCACTGGAA
Meis1 Forward: CAACACACACTTTACACACGCACG
Meis1 Reverse: TCAGGGTTATAAGGTGTCCCTTGG
Vax1 Forward: ATGTTCGGGAAACCAGACAAAATG
Vax1 Reverse: TCAGTCCAGCGCTTTTTTCTCG
Pbx3 Forward: GGATGGACGATCAATCCAGGATG
Pbx3 Reverse: GAGTTTGGCGTGGTGGGTGAG
TH Forward: GGAGGCTGTGGTATTCGAGG
TH Reverse: ACCAGTACACCGTGGAGAGT

Microscopy

Bright field images (in situ hybridization results) and some fluorescent images (Figs 3A–F′, 4A–L, 5A,B, and 8G,G′) were imaged with Olympus BX 51 microscope using a 4× or 10× objective. Other fluorescent images were taken with Olympus FV1000 confocal microscope system using 10×, 20×, 40×, or 60× objectives. Z-stack confocal images were reconstructed using the FV10-ASW software. All images were merged, cropped and optimized in Photoshop CS5 without distortion of the original information.

RNA-Seq

RNA-Seq analysis was performed as previously described (Zhang et al. 2016). The OBs from P11 *Sp8/Sp9-DCKO* mice and littermate controls (*Sp8/Sp9* floxed mice without *Dlx5/6-CIE*) (n = 2 mice, each group), and OBs from P30 *hGFAP-Cre*; $Sp8^{F/F}$; $Sp9^{F/F}$ mice and littermate controls were dissected (n = 4 mice, each group). In brief, total RNA was extracted using RNeasy Mini Kit (QIAGEN) according to the manufacturer's protocol, quantified using NanoDrop ND-2000, and checked for RNA integrity by an Agilent Bioanalyzer 2100 (Agilent Technologies, Santa Clara, CA, USA).

RNA-seq libraries were prepared according to the Illumina TruSeq protocol, quantified with Qubit 2.0 Fluorometer (Invitrogen), examined for dot distribution with Agilent 2100, and subjected to sequencing using Illumina Hiseq 2500. Acquired data were processed to obtain raw reads, which were then extracted for genome mapping with TopHat (version 2.0.9). Levels of gene expression were reported in FPKM (Trapnell et al. 2012). A gene was considered to be expressed if it had an FPKM > 1. For a gene to be called as differentially expressed, it required a $P < 0.05$. Data from this experiment has been deposited in the GEO database (GSE87417).

Quantification

Sp9 expression and its colocalization with DCX in the adult OB, RMS and V-SVZ (29 000 μm^2 area from the lateral V-SVZ) was quantified in 2–3 randomly chosen 30 μm sections from each mouse, and 3 adult mice were used.

Sp9 expression in the OB was quantified in 3 randomly chosen 12 μm sections for each mice (3 adult mice were used). We counted cells within a 400 000 μm^2 in the GCL, EPL, or glomerular layer per section. Quantification of interneuron subtypes in the OB was performed in the same way using P30 mice.

Quantification of $BrdU^+$, $Gsx2^+$, and $Ascl1^+$ cells in the dorsal–lateral V-SVZ (360 000 μm^2 per section) were performed in 30 μm coronal sections, and 3 sections from each mouse brain were analyzed. $BrdU^+$, $BrdU^+/DCX^+$, $Gsx2^+$, and $Ascl1^+$ cells per section in the RMS and OB core were quantified, and 3 sections from each brain were analyzed. Three mice were analyzed for each group.

For quantification of Ad-Cre labeled GFP^+ cells in the RMS and OB, about 5–9 30 μm coronal or sagittal sections were counted. Overall, 4–6 brains per group were analyzed.

The numbers of cleaved Caspase-3^+ cells were assessed in the V-SVZ, RMS, and OB (excluding the glomerular layer) of *Sp8/Sp9-DCKO* and control mice at P4, P7, and P11, and those of *hGFAP-Cre*; $Sp8^{F/F}$; $Sp9^{F/F}$ mice and littermate controls at P7 and P16. Of all, 9–12 40 μm sections of V-SVZ, RMS, or OB were quantified, 3 brains per group. We also counted cleaved Caspase-3^+ cells in the V-SVZ and RMS.

Statistics

Statistical significance was assessed using unpaired Student's t test. All quantification results were presented as the mean ± SEM (standard error of mean). P values less than 0.05 were considered significant.

Results

Sp9 is Widely Expressed in the Adult V-SVZ–RMS–OB System

We took advantage of a $Sp9^{LacZ}$ null allele that expresses β-galactosidase (Zhang et al. 2016) to analyze the expression of *Sp9* in the V-SVZ–RMS–OB system. X-gal staining demonstrated that *Sp9* is strongly expressed in the V-SVZ–RMS–OB in adulthood (Fig. 1A). Consistent with our previous report (Zhang et al. 2016), *Sp9* expression in the striatum and cortex was also observed (Fig. 1A). In the adult V-SVZ, 94.4% $Sp9^+$ cells expressed doublecortin (DCX), a marker of newly born neurons (neuroblasts), and about 90% DCX^+ cells expressed Sp9 (Fig. 1B–E). A small fraction of $Sp9^+$ and $Sp9^+/DCX^+$ cells also expressed Ascl1 (Zhang et al. 2016), consistent with the previous report that expression of this proneural transcription factor was retained in a small population of DCX^+ cells (Ponti et al. 2013).

Immunostaining showed that Sp8 and Sp9 are widely expressed in the adult OB; expression in the deep GCL was stronger for Sp9 than Sp8, whereas in the superficial GCL the reverse was observed with stronger Sp8 and weaker Sp9 expression (Supplementary Fig. S1A–C). Most $Sp9^+$ cells also expressed Sp8 and vice versa (Supplementary Fig. S1D–F″, K). About 50% CR^+ cells in the GCL and 88% CR^+ cells in the glomerular layer expressed Sp9 (Supplementary Fig. S1G, L). PV^+ cells in the EPL expressed Sp8 (Li et al. 2011), but not Sp9 (Supplementary Fig. S1J). We also found that Sp9 was expressed by less than 10% calbindin 1 $(CB)^+$ and TH^+ cells in the glomerular layer (Supplementary Fig. S1H, I, K).

No Major OB Neurogenesis Defects are Observed in *Sp9-KO* Mice

There was no significant difference in the sizes of OB between *Sp9-KO* mice and control littermates at P20 (Zhang et al. 2016), and the laminar organization of the OB was comparable (Fig. 1F–I′). We counted numbers of interneurons (CR^+, PV^+, CB^+, and TH^+ subtypes) in the *Sp9-KO* OB and control OB at P21, as

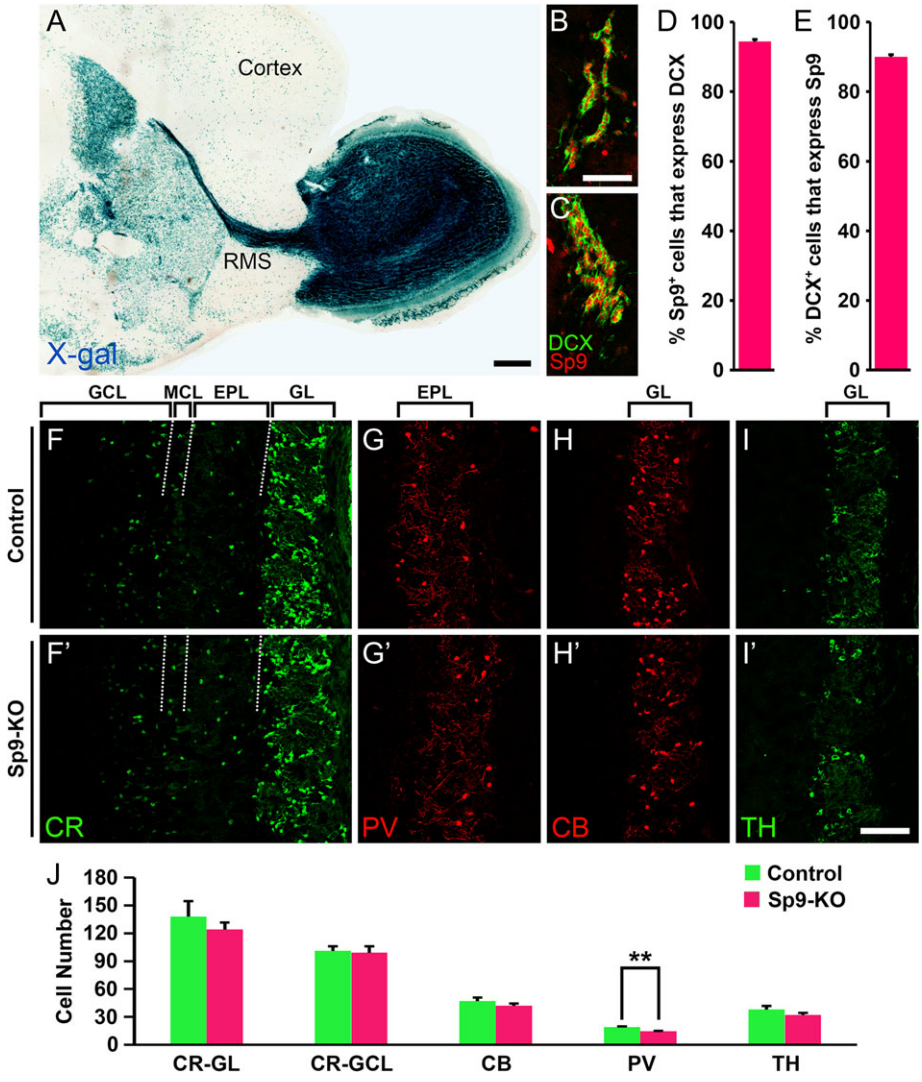

Figure 1. Sp9 is expressed in the DCX^+ neuroblasts in the adult V-SVZ. (*A*) An X-gal stained P30 $Sp9^{LacZ/+}$ mouse brain sagittal section showing strong *Sp9* expression in the V-SVZ–RMS–OB system. (*B–E*) The vast majority of DCX^+ V-SVZ cells expressed Sp9 and vice versa. $DCX^+/Sp9^+$ cells in the lateral (*B*) and dorsal lateral (*C*) V-SVZ are shown. (*F–J*) The numbers of CR^+, CB^+, and TH^+ cells were unaffected in the *Sp9-KO* OB at P21, except for PV^+ cells in the EPL, which showed a significant decrease. (Student's *t* test, $^{**}P < 0.01$, $n = 3$, mean ± SEM). EPL, external plexiform layer; GCL, granule cell layer; GL, glomerular layer; MCL, mitral cell layer. Scale bars: 500 μm in *A*; 50 μm in *B* for *B*, *C*; 100 μm in *I′* for *F–I′*.

most *Sp9-KO* mice die before or around P21 (Zhang et al. 2016). The numbers of CR^+, CB^+, and TH^+ neurons in the OB of *Sp9-KO* appeared normal. However the number of PV^+ cells in the EPL was significantly reduced (Fig. 1*J*). Thus, compared with the large number of OB interneuron loss in *Sp8-cKO* mice (Fig. 2*G–H″*) (Waclaw et al. 2006; Li et al. 2011), there was only a minor OB interneuron defect in *Sp9-KO* mice. Interestingly, we found that Sp8 expression was upregulated in the deep GCL of the *Sp9-KO* OB (Supplementary Fig. S1*M*, *N*), whereas Sp9 expression was not upregulated in the *Sp8-CKO* OB (data not shown).

Severe OB Interneuron Defects in *Sp8/Sp9-DCKO* Mice

The similar expression patterns of *Sp8* and *Sp9* in the V-SVZ–RMS–OB, and upregulation of Sp8 expression in the *Sp9-KO* OB suggest that they may play redundant roles in regulating OB interneuron development. Therefore, we analyzed neurogenesis in OBs of *Sp8/Sp9-DCKO* mice, in which *Sp8* and *Sp9* were deleted in all neuroblasts destined for the OB from embryonic to postnatal stage. *Sp8/Sp9-DCKO* mice developed weakness from birth and died between P5 and P12. Compared with *Dlx5/6-CIE* control OBs, *Sp8/Sp9-DCKO* OBs were severely reduced in size at P4 and P11 (Fig. 2*A–B′*). Accumulation of GFP^+ cells (*Dlx5/6-CIE*-expressing cells) in the central core of OB was observed in the mutants, compared with the normal laminar distribution of GFP^+ cells in the core to GCL, EPL and glomerular layer (Fig. 2*C–D′*). RNA in situ hybridization of *GAD1* confirmed that most GABAergic interneurons were restricted to the core of the OB in the *Sp8/Sp9-DCKO* mice at P11, with very few cells in the GCL and/or glomerular layer (Fig. 2*G″*). Moreover, $GAD1^+$ cells in the *Sp8/Sp9-DCKO* OBs were dramatically reduced compared with control and *Sp9-KO* OBs (Fig. 2*G*,*G′*,*G″*), and this reduction was also more pronounced than in *Sp8-CKO* OBs (Fig. 2*G″*). Notably, while *TH* mRNA expression was observed in OB superficial granule cells and periglomerular cells in controls, *Sp9-KOs* and *Sp8-CKOs*, we did not observe *TH* mRNA expression in *Sp8/Sp9-DCKOs* (Fig. 2*H–H″*), further suggesting that nearly all mature OB interneurons are lost in the absence of *Sp8/9* function. Taken together, *Sp8* and *Sp9* have redundant functions for OB interneuron development.

To analyze OB projection neurons, we performed in situ hybridization for *reelin* (*Reln*), which is mainly expressed by OB mitral/tufted cells (Hack et al. 2002). We found that $Reln^+$ cells were severely disorganized in the *Sp8/Sp9-DCKO* OB, as there was no clear distinction between the mitral cell layer, EPL and glomerular layer (Fig. 2*E–F′*). The density of $Reln^+$ cells was increased (Fig. 2*E–F′*), but the total number was unchanged at P11 indicating the increase of cell density was mostly due to the decrease in the OB volume. The numbers of $Reln^+$ cells per OB sections in the P11 *Sp8/Sp9-DCKO* mice (1133 ± 27 cells) and controls (1097 ± 53 cells) were similar (Student's *t* test, $P = 0.58$, $n = 3$), suggesting that the generation of OB projection neurons was not affected in *Sp8/Sp9-DCKO*.

Sp8 and *Sp9* Promote Neuronal Differentiation in the V-SVZ–RMS–OB

To investigate whether *Sp8* and *Sp9* are required for the transition from proliferating neural progenitors to neurons, we measured the numbers of $Gsx2^+$ and $Ascl1^+$ neural stem/progenitor cells in the V-SVZ–RMS–OB system of *Sp8/Sp9-DCKO* mice and control mice at P10. Compared with controls, there was a significant increase of $Gsx2^+$ and $Ascl1^+$ cells in the V-SVZ and OB of double mutants (Fig. 3*A–H*).

To further investigate the function of *Sp8* and *Sp9* in regulating OB interneuron development, we conditionally deleted *Sp8* and *Sp9* in V-SVZ neural stem cells using the *hGFAP-Cre* mouse (Zhuo et al. 2001). This transgenic line exhibits excision of floxed alleles in cortical radial glial cells starting around E12, and in the vast majority of neural stem cells in the postnatal and adult V-SVZ (Malatesta et al. 2003; Lim et al. 2009). Moreover, *hGFAP-Cre* is not active in the ventral LGE until later stages of development (Malatesta et al. 2003). Therefore, by the time *Sp8* and *Sp9* are inactivated in *hGFAP-Cre*; $Sp8^{F/F}$; $Sp9^{F/F}$ mice, the striatum is well developed and a substantial number of OB interneurons have been generated. In contrast to *Sp8/Sp9-DCKO* mice, which died between P5 and P12, the growth and survival of *hGFAP-Cre*; $Sp8^{F/F}$; $Sp9^{F/F}$ mice were indistinguishable from littermate control mice (i.e., $Sp8^{F/F}$; $Sp9^{F/F}$).

To measure the number of cells in S-phase of the cell cycle, we injected BrdU into adult (P60) *hGFAP-Cre*; $Sp8^{F/F}$; $Sp9^{F/F}$ mice, and quantified the numbers of proliferating cells in the V-SVZ–RMS–OB 1 h after BrdU injection. Compared with controls, we observed more $BrdU^+$ cells in the mutant V-SVZ and RMS (Supplementary Fig. S2*A–B′*, *K*). Notably, cycling cells in the core of the OB appeared to be more prominent. Very few $BrdU^+$ and $BrdU^+/DCX^+$ cells were observed in the control OB in adult mice (Supplementary Fig. S2*C*, *J*). In contrast, the OBs of *hGFAP-Cre*; $Sp8^{F/F}$; $Sp9^{F/F}$ mice showed an approximately 16-fold and 60-fold increase in the number of $BrdU^+$ and $BrdU^+/DCX^+$ cells, respectively (Supplementary Fig. S2*C′*, *J′*, *K*, *L*). Consistent with this observation, an increase of $Gsx2^+$ and $Ascl1^+$ progenitor cells was also observed in the V-SVZ–RMS–OB of mutant mice (Supplementary Fig. S2*D–I*'). Again, whereas $Gsx2^+$ and $Ascl1^+$ cells were rare in the adult control OBs (Supplementary Fig. S2*F*, I), $Gsx2^+$ and $Ascl1^+$ cells were greatly increased in the OB core of *hGFAP-Cre*; $Sp8^{F/F}$; $Sp9^{F/F}$ mice (Supplementary Fig. S2*F′*, *I′*, *M*, *N*). Homeodomain transcription factor Gsx2 and proneural transcription factor Ascl1 have been shown to promote neural progenitor proliferation in the embryonic and adult brain (Bertrand et al. 2002; Castro et al. 2011; Pei et al. 2011; Lopez-Juarez et al. 2013; Andersen et al. 2014; Imayoshi and Kageyama 2014), whereas Sp8 and Sp9 are mainly expressed by neuroblasts and mature OB interneurons (Fig. 1*A–E*) (Waclaw et al. 2006; Liu et al. 2009). Therefore, the increased numbers of $Gsx2^+$, $Asc1^+$, and $BrdU^+$ cells in the V-SVZ–RMS–OB in *Sp8/Sp9* double mutants suggest that the process for the neural progenitors to generate immature neurons, at least partly, was blocked.

Neuroblasts Migration Defects in the *hGFAP-Cre*; $Sp8^{F/F}$; $Sp9^{F/F}$ Mice

Although neuronal differentiation was inhibited, substantial neuroblasts were still produced in the V-SVZ–RMS–OB of *Sp8/Sp9* double mutant mice (e.g., $BrdU^+$ and $BrdU^+/DCX^+$ cells were seen in the mutant OBs, Supplementary Fig. 2*J*, *J′*). We then examined neuroblast migration in the lateral wall of the lateral ventricle using whole-mount staining (Doetsch and Alvarez-Buylla 1996; Mirzadeh et al. 2010). DCX^+ neuroblasts are organized in chains in the SVZ of adult (P90) *hGFAP-Cre*; $Sp8^{F/F}$; $Sp9^{F/F}$ mice similar to those observed in controls (Fig. 4*A*,*B*). Strikingly, however, there was an obvious increase in these neuroblast chains in mutant mice (Fig. 4*A*,*B*). Furthermore, these chains appeared disoriented in *hGFAP-Cre*; $Sp8^{F/F}$; $Sp9^{F/F}$ mice compared with controls, as many were oriented perpendicular to the RMS in the anterior wall (Fig. 4*B*), indicative of a disturbance in tangential migration ($n = 4$ mice per group).

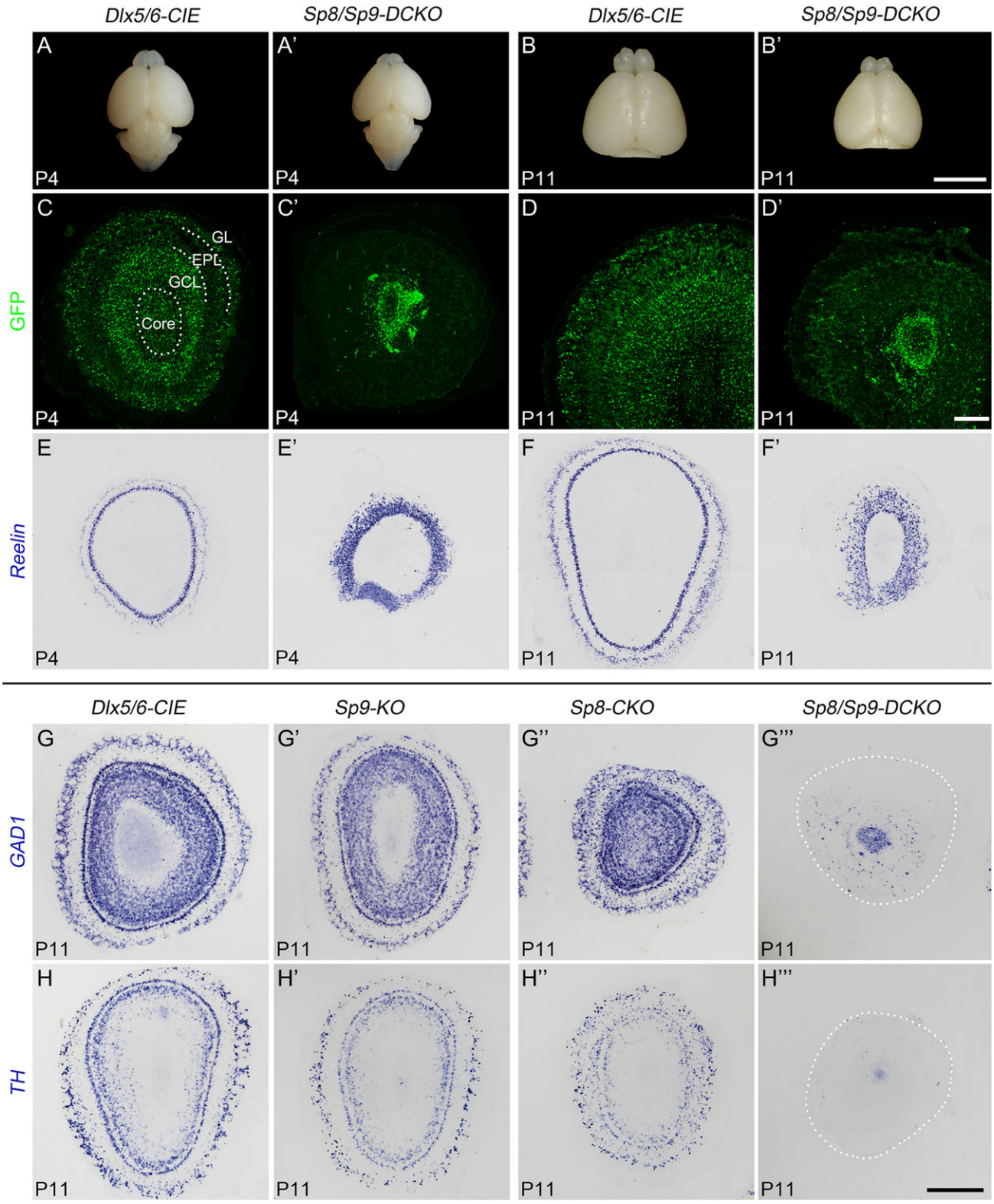

Figure 2. Severely reduced OB interneurons in *Sp8/Sp9-DCKO* mice. (*A–B′*) The OBs and telencephalons from *Sp8/Sp9-DCKO* mice were smaller than *Dlx5/6-CIE* controls at P4 and P11. (*C–F′*) GFP immunostaining and *Reln* in situ RNA hybridization on P4 and P11 OB sections. Note that most GFP$^+$ cells were restricted to the core of the OB in *Sp8/Sp9-DCKO* mice. (*G–H‴*) *GAD1* and *TH* in situ RNA hybridization on P11 OB sections of control, *Sp9-KO*, *Sp8-CKO* and *Sp8/Sp9-DCKO* mice. *TH* mRNA was not detected in *Sp8/Sp9-DCKO* OBs. EPL, external plexiform layer; GCL, granule cell layer; GL, glomerular layer. Scale bars: 5 mm in *B′* for *A–B′*; 200 μm in *D′* for *C–D′*; 500 μm in *H‴* for *E–H‴*.

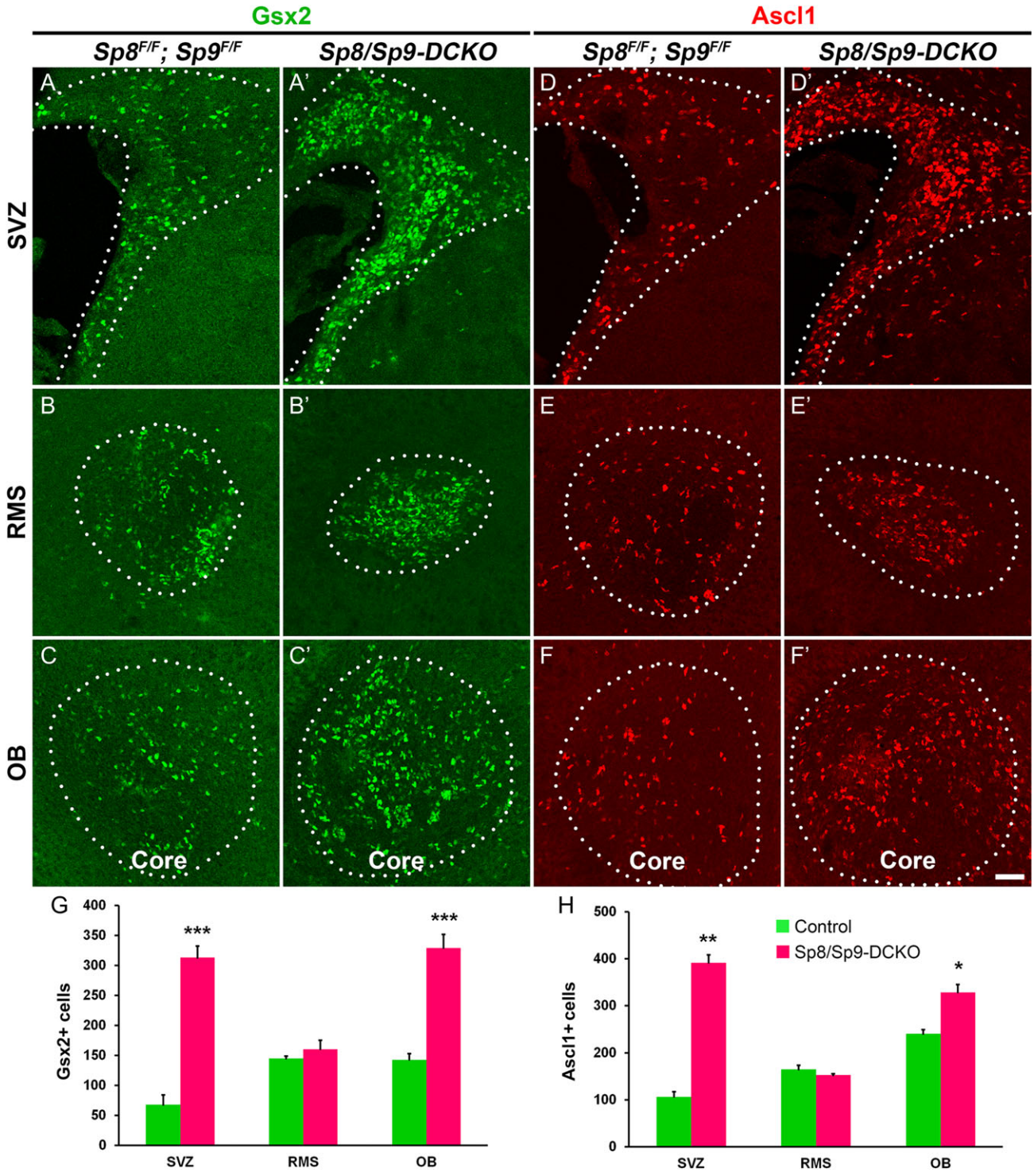

Figure 3. Neural stem/progenitor cells accumulate in the V-SVZ and OB of postnatal *Sp8/Sp9*-DCKO mice. (*A*–*F*′) Representative images of Gsx2$^+$ and Ascl1$^+$ cells in the V-SVZ–RMS–OB of the control and *Sp8/Sp9*-DCKO mice at P10. (*G*, *H*) The numbers of Gsx2$^+$ and Ascl1$^+$ cells in the V-SVZ and OB were significantly increased in *Sp8/Sp9*-DCKO mice compared with controls. (Student's *t* test, $^*P < 0.05$, $^{**}P < 0.01$, $^{***}P < 0.001$, $n = 3$, mean ± SEM). Scale bar: 50 μm.

The sizes of OBs were reduced in adult *hGFAP-Cre*; *Sp8*$^{F/F}$; *Sp9*$^{F/F}$ mice and the numbers of neurons within OB were significantly decreased compared with littermate controls (Fig. 4E–H). The laminar structures (i.e., GCL, EPL, and glomerular layers) of the OB were largely preserved in the mutants, as shown by NeuN (Rbfox3, a mature neuron marker), but not as clearly defined as those in the control mice (Fig. 4E,F). DCX$^+$ neuroblasts were observed in the *hGFAP-Cre*; *Sp8*$^{F/F}$; *Sp9*$^{F/F}$ OB, but based on their orientations, most of them were not able to switch from tangential to radial migration (Fig. 4J,N). As a result the DCX$^+$ mutant cells were largely restricted to the OB core with very few present within the GCL or more superficial layers

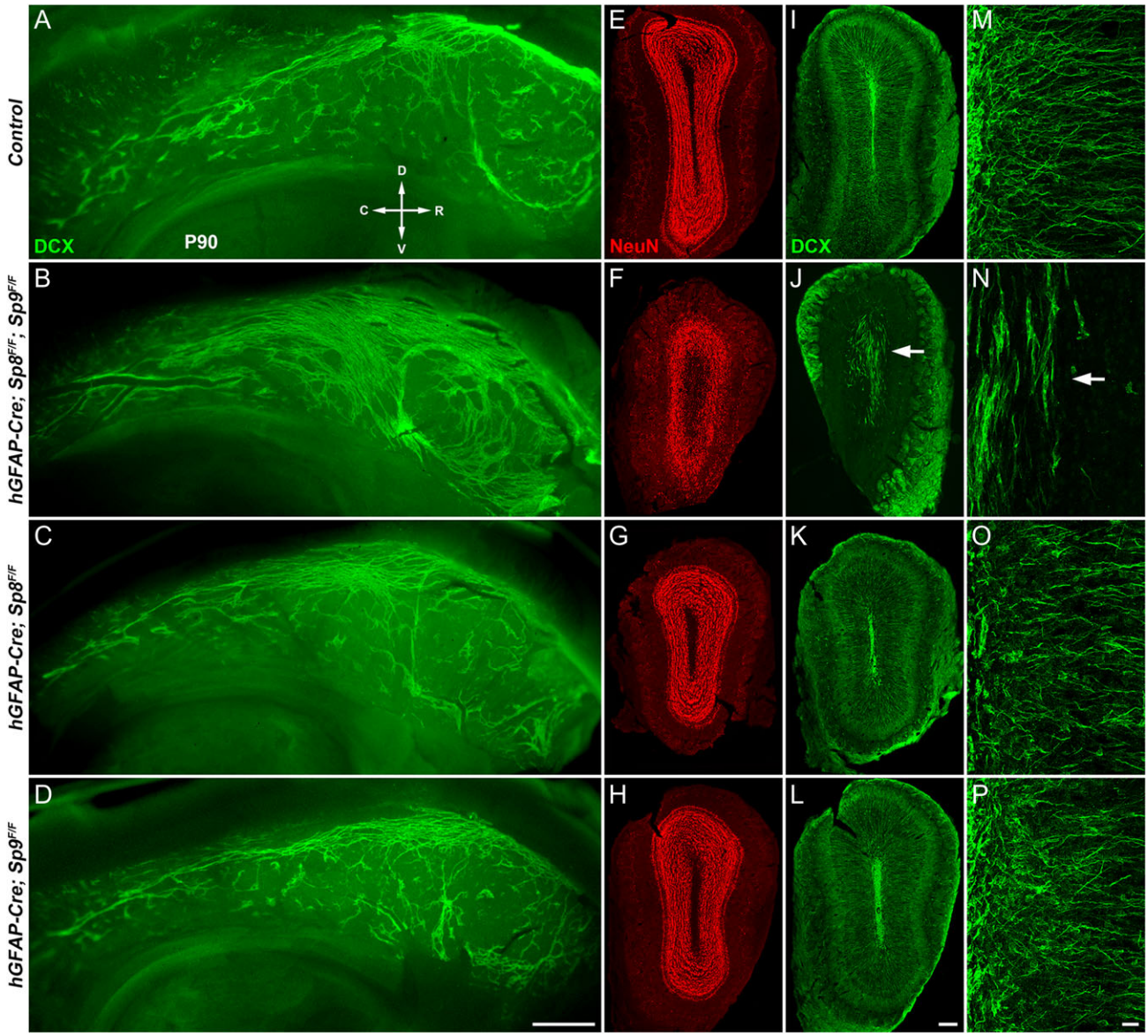

Figure 4. Tangential and radial migration defects of neuroblasts in adult *hGFAP-Cre*; $Sp8^{F/F}$; $Sp9^{F/F}$ mice. (*A–D*) Whole mount of the lateral wall of the lateral ventricle stained with antibody against DCX showed a marked increase in neuroblast chains in double mutants at P90. (*E–L*) P90 OB coronal sections stained for NeuN and DCX. Note that *hGFAP-Cre*; $Sp8^{F/F}$; $Sp9^{F/F}$ double mutant OBs were smaller than control, *hGFAP-Cre*; $Sp9^{F/F}$ and *hGFAP-Cre*; $Sp8^{F/F}$ OBs. (*M–P*) High magnification images of DCX^+ cells in OBs. Arrows indicate defects in radial migration of neuroblasts. R, rostral; C, caudal; D, dorsal; V, ventral. Scale bars: 500 μm in (*D*) for (*A–D*); 200 μm in (*L*) for (*E–L*); 20 μm in (*P*) for (*M–P*).

(Fig. 4*I–P*). Note that although *hGFAP-Cre*; $Sp8^{F/F}$; $Sp9^{F/F}$ OBs have many more $Gsx2^+$, $Asc1^+$, $BrdU^+$, $BrdU^+/DCX^+$ cells, the number of neuroblasts was severely reduced compared with controls (Fig. 4*M–P*, Supplementary Fig. S2), further suggesting an inhibition of neuronal differentiation. This in conjunction with defects in neuroblast tangential and radial migration, shows that *Sp8/9* are required at multiple steps in the generation and migration of OB interneurons.

We did not observe defects of neuroblast tangential migration in the lateral wall of the lateral ventricle in *Sp8* or *Sp9* single mutants (Fig. 4*C,D*). There were also no visible defects of neuroblast radial migration in single mutant OBs (Fig. 4*K,L,O,P*). These results strongly suggest that *Sp8* and *Sp9* together are required for the tangential and radial migration of young neurons from the SVZ to different layers of the OB.

Sp8/9-deficent Neuroblasts Have a Cell-Autonomous Defect in Tangential and Radial Migration in the V-SVZ–RMS–OB System

To directly assess neuroblast tangential and radial migration, we injected Cre recombinase-expressing adenovirus (Ad-Cre) into the dorsolateral SVZ of P0 *Rosa-YFP* control and $Sp8^{F/F}$; $Sp9^{F/F}$; *Rosa-YFP* mice. Direction of migration was determined based on the orientation of the leading process (Sawamoto et al. 2006). In control experiments, by 1 week after Ad-Cre injection, GFP^+ neuroblasts reached the OB and some of them had switched from tangential to radial migration (Fig. 5*A*). This is consistent with previous observations (Petreanu and Alvarez-Buylla 2002; Sawamoto et al. 2006). On the other hand, while in the mutants ($Sp8^{F/F}$; $Sp9^{F/F}$; *Rosa-YFP* mice),

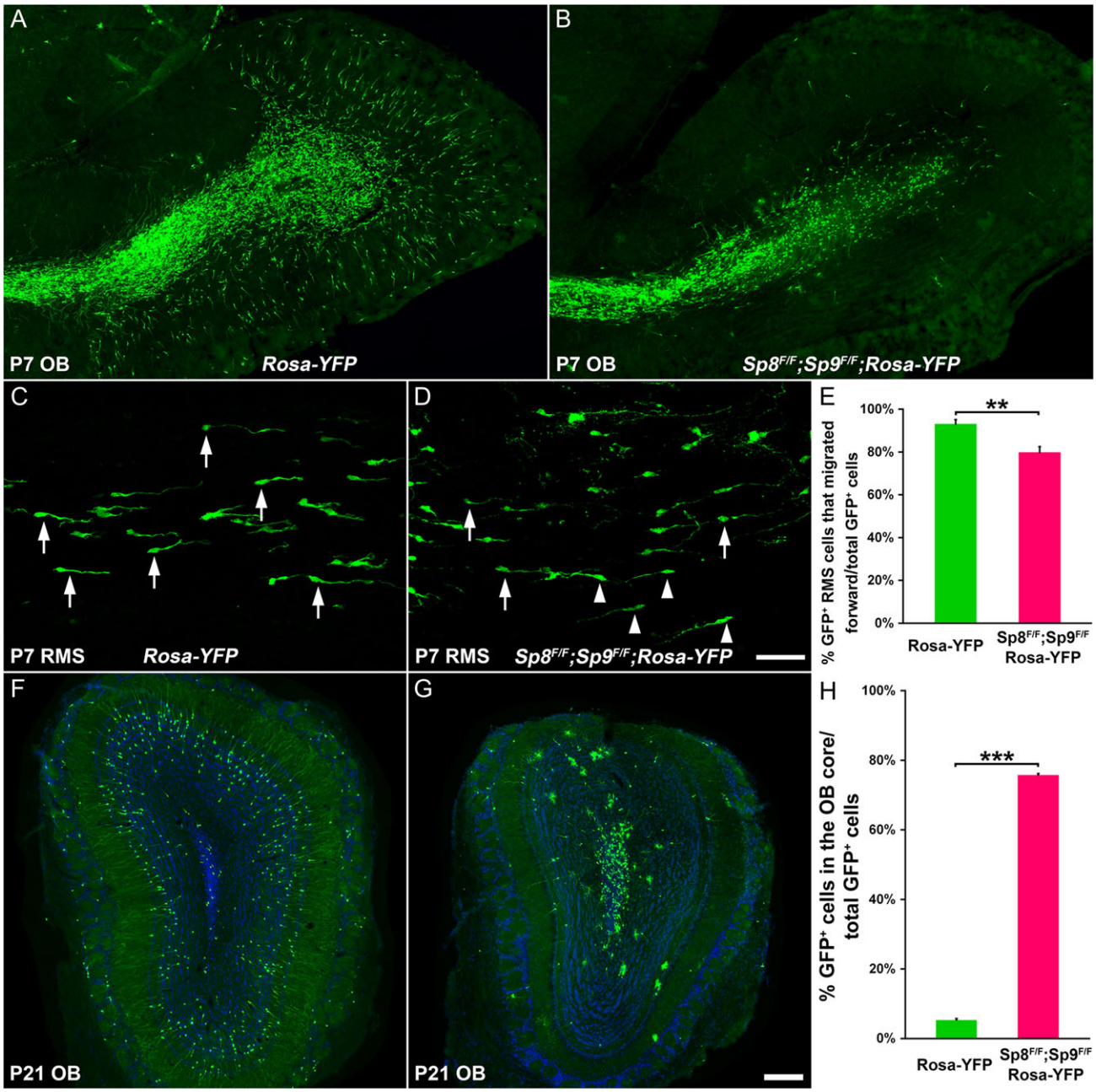

Figure 5. *Sp8* and *Sp9* are required cell autonomously for neuroblast tangential and radial Migration. (*A*, *B*) *Sp8* and *Sp9* were deleted by injecting Ad-Cre into the P0 dorsolateral V-SVZ. GFP$^+$ cells in the P7 OB of *Rosa-YFP* and *Sp8*$^{F/F}$; *Sp9*$^{F/F}$; *Rosa-YFP* mice were shown. (*C*, *D*) GFP$^+$ migratory neuroblasts in the P7 RMS. Arrows indicate cells oriented in the direction of the OB, whereas arrowheads indicate cells oriented in the reverse direction. (*E*) Quantification of the percentage of GFP$^+$ cells oriented in the forward direction. (Student's *t* test, $^{**}P < 0.01$, $n = 4$, mean ± SEM). (*F*, *G*) GFP$^+$ cells in the P21 OB of *Rosa-YFP* and *Sp8*$^{F/F}$; *Sp9*$^{F/F}$; *Rosa-YFP* mice are shown. (*H*) Quantification of the percentage of GFP$^+$ cells that were in the OB core. (Student's *t* test, $^{**}P < 0.001$, $n = 3$, mean ± SEM). Scale bars: 200 μm in (*G*) for (*A*, *B*, *F*, *G*); 50 μm in (*D*) for (*C*, *D*).

some GFP$^+$ neuroblasts also reached the OB, most of them failed to switch from tangential to radial migration (Fig. 5*B*). In the RMS of control mice, 93% GFP$^+$ cells were oriented in the forward direction (the direction of the OB) (Fig. 5*C*,*E*), whereas, this number was 79% in the RMS of *Sp8*$^{F/F}$; *Sp9*$^{F/F}$; *Rosa-YFP* mice (Fig. 5*D*,*E*). Therefore, loss of *Sp8* and *Sp9* function resulted in disorientation of tangentially migrating neuroblasts.

Three weeks after Ad-Cre injection, we counted the number of GFP$^+$ cells in the OB. In the control mice, most GFP$^+$ in the OB dispersed in the GCL and glomerular layers (Fig. 5*F*,*H*). Some GFP$^+$ cells in the GCL showed branched dendrites and dendritic spines, typical features of mature OB granular cells (Fig. 5*F*) (Petreanu and Alvarez-Buylla 2002). In contrast, 76% of *Sp8*/9-deficient GFP$^+$ cells that reached the OB remained in the core; only a small fraction of GFP$^+$ cells were observed in the GCL and glomerular layer (Fig. 5*G*,*H*). Taken together, these results suggest that *Sp8* and *Sp9* are essential for both the tangential and radial migration of neuroblasts in the V-SVZ–RMS–OB system in a cell-autonomous manner.

Apoptotic Cell Death is Increased in the V-SVZ–RMS–OB of Postnatal *Sp8/Sp9-DCKO* Mice

We performed cleaved Caspase-3 immunostaining to examine whether cell death contributed to the reduction of immature and mature interneurons in the OB of *Sp8/Sp9-DCKO* mice. At all postnatal stages analyzed (P4, P7, and P11), we found increased number of Caspase-3$^+$ cells in the V-SVZ, RMS and OB of *Sp8/Sp9-DCKO* mice compared with littermate controls (*Sp8/Sp9* floxed mice without *Dlx5/6-CIE*) (Fig. 6A–*I*). The increase in Caspase-3$^+$ cells in the mutant OB was most evident in core (Fig. 6F), where most *GFP*$^+$ and *GAD1*$^+$ cells were located (Fig. 2*C*′, *D*′,*G*″′). There were also more Caspase-3$^+$ cells in the V-SVZ, RMS and OB of *hGFAP-Cre*; *Sp8*$^{F/F}$; *Sp9*$^{F/F}$ mice compared with controls at P7 and P16 (Supplementary Fig. S3A–*I*). Increased apoptosis in the adult V-SVZ, RMS, and OB of *hGFAP-Cre*; *Sp8*$^{F/F}$; *Sp9*$^{F/F}$ mice continued to be observed, but was less conspicuous than that in the younger mice (Supplementary Fig. S3G–*I*). Thus, *Sp8* and *Sp9* are required to promote cell survival in the V-SVZ–RMS–OB system. Consistent with our previous finding that *Sp9* promotes the survival of postmitotic striatopallidal projection neurons (Zhang et al. 2016), increased apoptotic cell death was also found in the *Sp8/Sp9* double mutant striatum (Fig. 6A,*B*; Supplementary Fig. S3A, *B*).

RNA-Seq Analysis Reveals Key Molecular Defects in the OBs of *Sp8/Sp9-DCKO*

To characterize the molecular changes in the OBs of *Sp8/Sp9-DCKO* mice, we performed RNA-Seq analysis. We compared gene expression profiles from P11 OB of *Sp8/Sp9-DCKO* mice to those of littermate controls ($n = 2$ biological replicas, GEO accession number: GSE87417). Gene expression levels were reported in FPKM (fragments per kilobase of exon per million fragments mapped) (Trapnell et al. 2012). For example, the expression levels (FPKM) of *Sp8* and *Sp9* genes in P11 control OB were 30.3 and 24.9, respectively. Whereas, in *Sp8/Sp9-DCKO* OBs at P11, *Sp8* and *Sp9* gene expression levels were reduced to 1.8 and 0.1 (Supplementary Table 1) demonstrating that the mutation effectively reduced OB expression of *Sp8* and *Sp9*.

To study the impact of *Sp8/Sp9* double deletion on different cell types in the OB, such as neural stem/progenitors in the OB core, mitral/tufted cells, astrocytes, and interneurons, we explored expression levels for genes that are enriched in these populations (Supplementary Table S1, S2). We found that RNA levels of OB interneuron-enriched genes were either significantly reduced (fold change, 0.15–0.3, mutants vs. controls), such as *Dlx1*, *Dlx2*, *Dlx5*, *Dlx6*, *Etv1* (*Er81*), *Gad1*, *Gad2*, *Meis2*, *Neto1*, *Pbx1*, *Pbx3*, *Rbfox3*, and *Tshz1* (Supplementary Table S1),

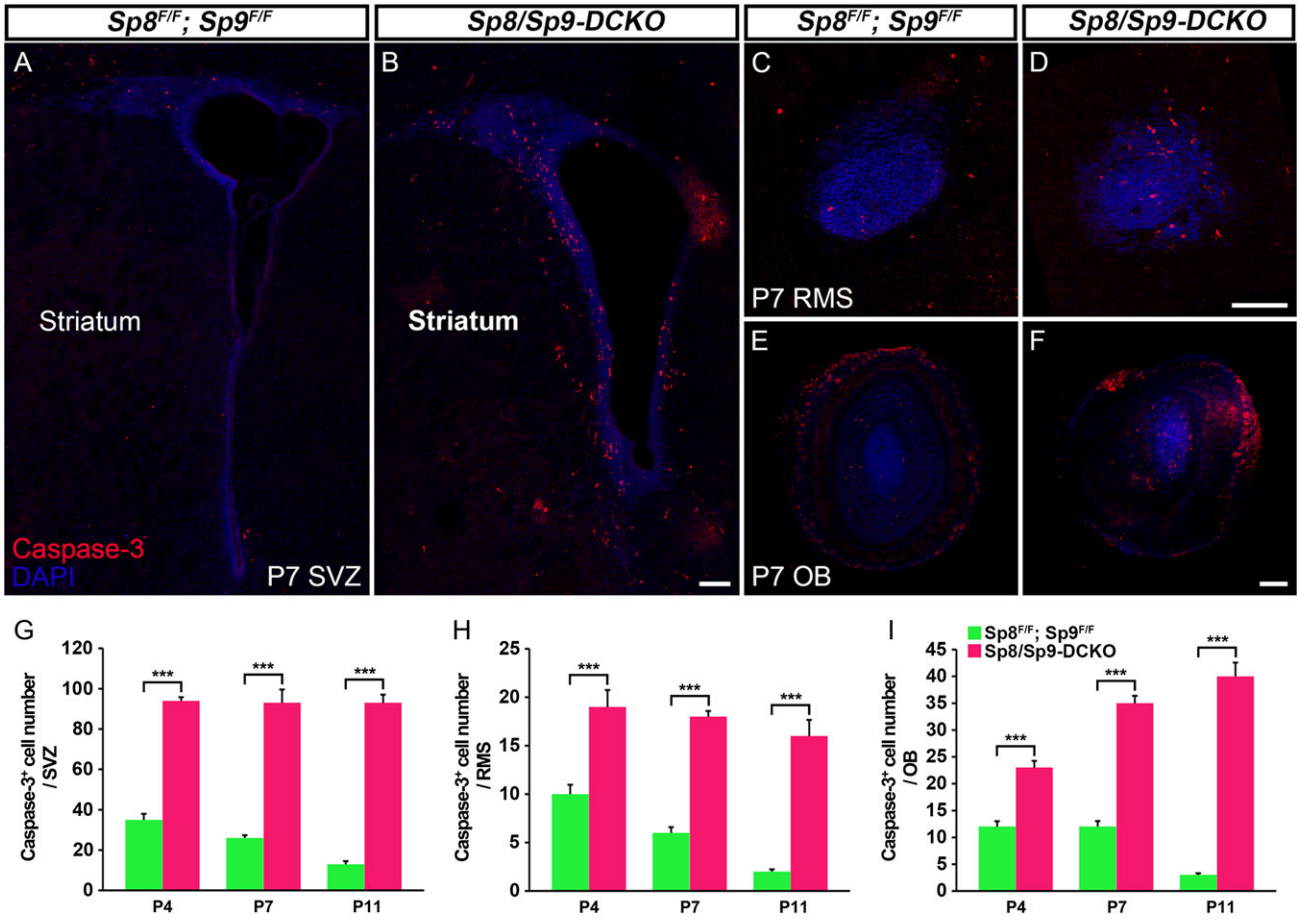

Figure 6. Apoptotic cells are significantly increased in the V-SVZ, RMS and OB in *Sp8/Sp9-DCKO* mice. (A–F) Cleaved Caspase-3$^+$ cells in the V-SVZ–RMS–OB of controls and double mutants at P7. (G–*I*) Numbers of Caspase-3$^+$ cells in the mutant V-SVZ, RMS and OB were significantly higher than those in controls at P4, P7, and P11. (Student's *t*-test, $^{***}P < 0.001$, $n = 3$, mean ± SEM). Scale bars: 100 μm in *B* for *A*, *B*; 100 μm in *D* for *C*, *D*; 200 μm in *F* for *E*, *F*.

or nearly undetectable, such as *Meis1*, *Prokr2*, and *Vax1* (0.6, 0.5, and 0.27, FPKM, respectively) (Supplementary Table S1).

In contrast, transcription factors that are expressed in neural stem/progenitors for OB interneurons, such as *Gsx1*, *Gsx2*, *Nr2e1 (Tlx)*, and *Ascl1*, were slightly increased (Supplementary Table S2). Increased expressions of *Gsx2* and *Ascl1* revealed by RNA-seq was consistent with our immunostaining results (Fig. 3C,C′,F–H), which supported our proposal that in the *Sp8/Sp9-DCKO* neural stem/progenitors have reduced neurogenesis. The expression of mitral/tufted cell markers [*Eomes (Tbr2)*, *Reln*, *Slc176a (Vglut2)*, *Slc17a7 (Vglut1)*, *Tbr1* and *Tbx21*], and the astrocyte markers [*Aldoc*, *Aldh1l1*, *Aqp4*, *Fabp5*, *Fabp7 (Blbp)*, *GFAP*, *Gja1 (Cx43)*, *S100b*, *Slc1a3 (Glast1)*, and *Vim (Vimentin)*] were all significantly increased, levels ranging from a 1.5 to 4-fold change (Supplementary Table S2). We posit that this is largely due to the loss of interneurons, which changed the relative ratio of OB cell types. These RNA-Seq results further confirmed that decreased interneuron genesis was the most salient feature in the OB of *Sp8/Sp9-DCKO* mice.

Sp8/Sp9-DCKO dLGE Fail to Express *Tshz1* and *Prokr2*

Prokineticin 2 (*PROK2*) and *PROKR2* signaling is required for the neuronal differentiation, neuronal migration from the SVZ through the RMS to their final layers in the OB and cell survival; defects in this signaling result in Kallmann syndrome in humans (Ng et al. 2005; Dode et al. 2006; Matsumoto et al. 2006; Pitteloud et al. 2007; Prosser et al. 2007; Sarfati et al. 2010; Martin et al. 2011; Ragancokova et al. 2014). A recent study has shown that *Tshz1* is required for neuronal differentiation, and is essential for neuroblast radial migration in the OB in part through directly promoting *Prokr2* expression (Ragancokova et al. 2014). Our RNA-Seq analysis revealed that *Prokr2* expression was lost and *Tshz1* expression was significantly downregulated in the *Sp8/Sp9-DCKO* mouse OB (Supplementary Table S1). Moreover, removal of *Sp8* and *Sp9* in the V-SVZ–RMS–OB of *Sp8/Sp9-DCKO* and *hGFAP-Cre*; $Sp8^{F/F}$; $Sp9^{F/F}$ mice led to phenotypes similar to those observed in *Prok2*, *Prokr2*, and *Tshz1* constitutive or conditional mutants: reduction in OB size, loss of normal OB architecture, blockage of neuronal differentiation, defect in the tangential and radial migration of young interneurons, and increased cell death in the V-SVZ–RMS–OB (Ng et al. 2005; Matsumoto et al. 2006; Prosser et al. 2007; Ragancokova et al. 2014). Therefore, we next examined the expression of *Prokr2* and *Tshz1* in the V-SVZ, RMS, and OB of *Sp9-KO*, *Sp8-CKO*, and *Sp8/Sp9-DCKO* mice.

To study the roles of *Sp8* and *Sp9* in regulating *Prokr2* and *Tshz1* expression, we performed in situ RNA hybridization in control, *Sp9-KO*, *Sp8-CKO*, and *Sp8/Sp9-DCKO* mice. During embryonic development, the dLGE and RMS are the main source of OB interneurons (Stenman et al. 2003; Waclaw et al. 2006; Long et al. 2007). Consistent with this, we observed that *Prokr2* and *Tshz1* were expressed in the dLGE but not in the ventral LGE of control mice at E16.5 (Fig. 7A,B). There were no visible differences in the expression of *Tshz1* and *Prokr2* in the *Sp9-KO* dLGE compared with controls (Fig. 7A′,B′), while their expression levels in the dLGE of the *Sp8-CKO* were reduced (Fig. 7A″,B″). Interestingly, complete loss of *Tshz1* and *Prokr2* expression was observed in the dLGE of *Sp8/Sp9-DCKO* mice (Fig. 7A‴,B‴). Similarly, the expression of *Prokr2* and *Tshz1* in the RMS and OB, was greatly reduced or undetectable in the double mutants (Fig. 7C–F‴). A recent study shows that *Tshz1* is also expressed in mitral/tufted cells (Kawasawa et al. 2016). Thus, the *Tshz1* expression remaining in the *Sp8/Sp9-DCKO* OB (Fig. 7F‴) likely represents mitral/tufted cells, as marked by *Reln* in the double mutants (Fig. 2E–F′).

Tshz1 and *Prokr2* Expression in the Postnatal V-SVZ–RMS–OB Depends on Sp8 and Sp9

In the postnatal brain, OB interneurons are derived from neural stem/progenitor cells in the lateral, dorsal (cortical), and medial (septal) V-SVZ (Vergano-Vera et al. 2006; Kohwi et al. 2007; Merkle et al. 2007, 2014; Young et al. 2007; Alonso et al. 2008). Accordingly, we observed *Prokr2* and *Tshz1* expression in the lateral, dorsal, and medial V-SVZ, as well as in the RMS and OB in coronal and sagittal sections of control mice at P4 (Fig. 8A–I). This is consistent with previous observations that most neuroblasts in the V-SVZ–RMS–OB system express *Prokr2* and *Tshz1* (Ng et al. 2005; Ragancokova et al. 2014). The expressions of *Prokr2* and *Tshz1* in the V-SVZ–RMS–OB in *Sp9-KO* and control mice were comparable, while the *Sp8-CKO* showed reduced expression of *Prokr2* and *Tshz1* (Fig. 8A–F″). Again, the expression of *Prokr2* and *Tshz1* in *Sp8/Sp9-DCKO* mice was undetectable, except for the presumed *Tshz1* expression in mitral/tufted cells (Fig. 8A–I′). Interestingly, while we observed only subtle defects in *Sp9-KO* OB interneurons, there were more $Prokr2^{+}$ and $Tshz1^{+}$ cells in the *Sp9-KO* SVZ (Fig. 8A′,B′). This probably is due to atrophy of the striatum as most striatopallidal neurons are lost in *Sp9-KO* mice (Zhang et al. 2016).

To confirm our RNA-Seq results from P11 OBs (Supplementary Table S1), we have also examined *Tshz1* and *Prokr2* expression in the V-SVZ, RMS and OB in these mice at P11, and found the expression patterns nearly identical to those observed in P4 mice (Supplementary Fig. S4A–F‴).

Finally, we examined *Tshz1* and *Prokr2* expression in control and *hGFAP-Cre*; $Sp8^{F/F}$; $Sp9^{F/F}$ mice at P21. *Tshz1* and *Prokr2* expression in the mutant RMS was barely detectable compared with controls which displayed strong staining (Supplementary Fig. S5D–G′). Of note, while *Tshz1* expression was retained in a subpopulation of interneurons and mitral/tufted cells in *hGFAP-Cre*; $Sp8^{F/F}$; $Sp9^{F/F}$ mice, its expression in the OB core was significantly downregulated (Supplementary Fig. S5A–B′), suggesting loss of *Tshz1* expression in newly born neuroblasts, consistent with its expression pattern in the RMS (Supplementary Fig. S5F′). *Prokr2* is a G protein-coupled receptor of chemokine *Prok2*, and its signaling promotes the neuroblast migration. Therefore, *Prokr2* expression is downregulated in mature OB interneurons when these cells stop migrating (Supplementary Fig. S5C). Indeed, although a subpopulation of DCX^{+} neuroblasts within the core and $NeuN^{+}$ interneurons in each layer were present in the OB (Fig. 4E–P), we observed very few $Prokr2^{+}$ cells in the P21 OB of *hGFAP-Cre*; $Sp8^{F/F}$; $Sp9^{F/F}$ mice (Supplementary Fig. S5C′).

We also performed RNA-Seq to compare gene expression profiles from P30 OB of *hGFAP-Cre*; $Sp8^{F/F}$; $Sp9^{F/F}$ mice to those of littermate controls (n = 4 biological replicas, GEO accession number: GSE87417). Consistent with the RNA-Seq data from P11 *Sp8/Sp9-DCKO* mouse OB, interneuron specific gene expression levels showed an 2–3-fold decrease in the *hGFAP-Cre*; $Sp8^{F/F}$; $Sp9^{F/F}$ mouse OB compared with controls (Supplementary Table S3, S4). We found that the expression level of *DCX* gene in control OB was 81.7 (FPKM), whereas it was reduced to 24.7 in the mutant OB (fold change: mutants vs. control, 0.30) (Supplementary Table S3). The expression level of *Prokr2* gene in control OBs was 11.1, however, in P30 *hGFAP-Cre*; $Sp8^{F/F}$; $Sp9^{F/F}$ mouse OB, *Prokr2* gene expression level was reduced to 0.5 (fold change: 0.04) (Supplementary Table S3). This result further suggests that Sp8/9 promote *Prokr2* expression in the OB.

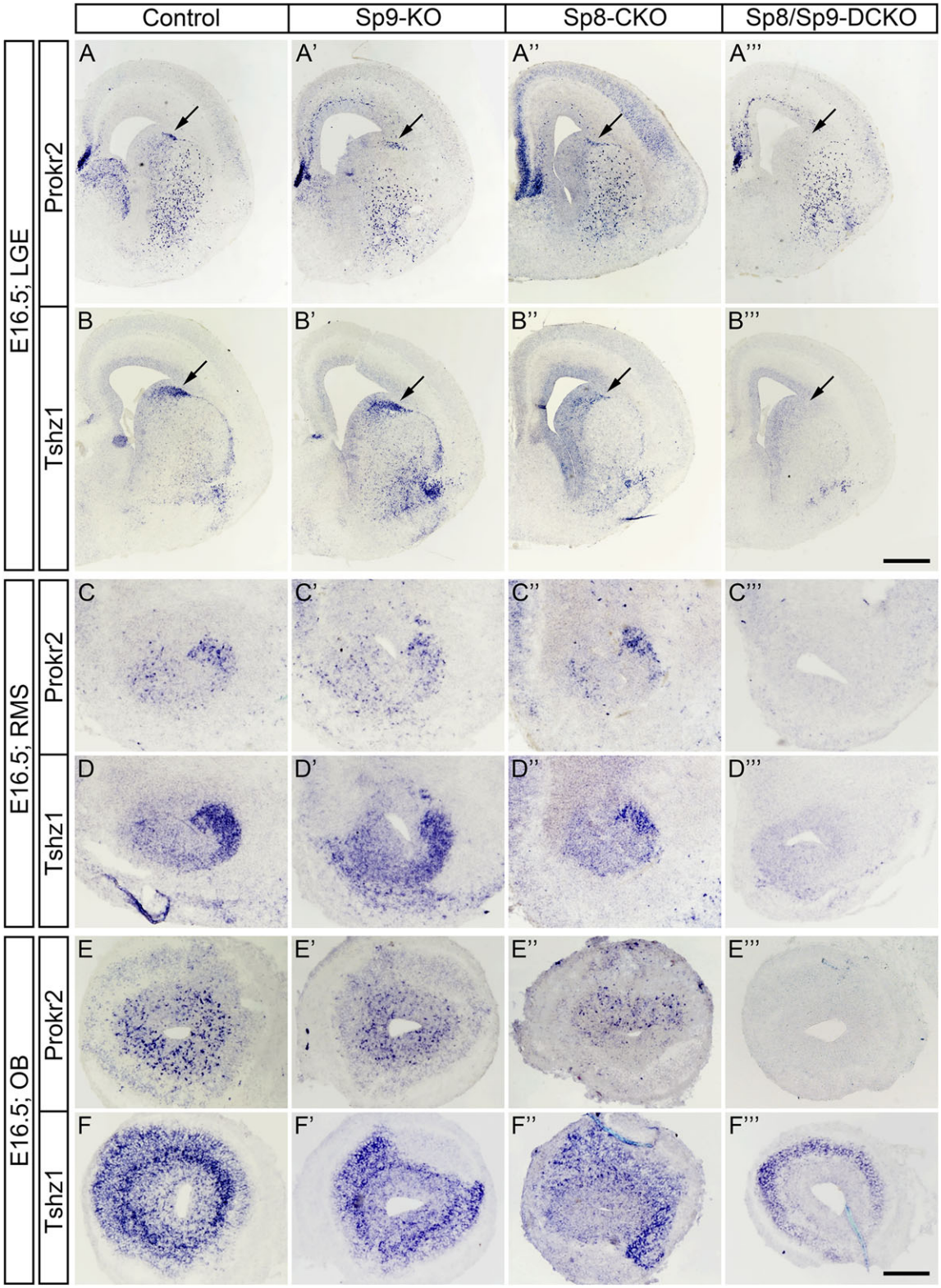

Figure 7. *Sp8/Sp9*-DCKO mice fail to express *Prokr2* and *Tshz1* in the embryonic dLGE, RMS and OB. (*A–F‴*) Expression of *Prokr2* and *Tshz1* were absent in the E16.5 dLGE (arrows), RMS and OB of *Sp8/Sp9-DCKO*. There were no visible differences in the expression of *Tshz1* and *Prokr2* in the *Sp9-KO* compared with controls while in *Sp8-CKO* was slightly reduced (*A″*, *B″*). Note that *Tshz1* expression in mitral/tufted cells was unaffected (*F‴*). Scale bars: 500 μm in *B‴* for *A–B‴*; 200 μm in *F‴* for *C–F‴*.

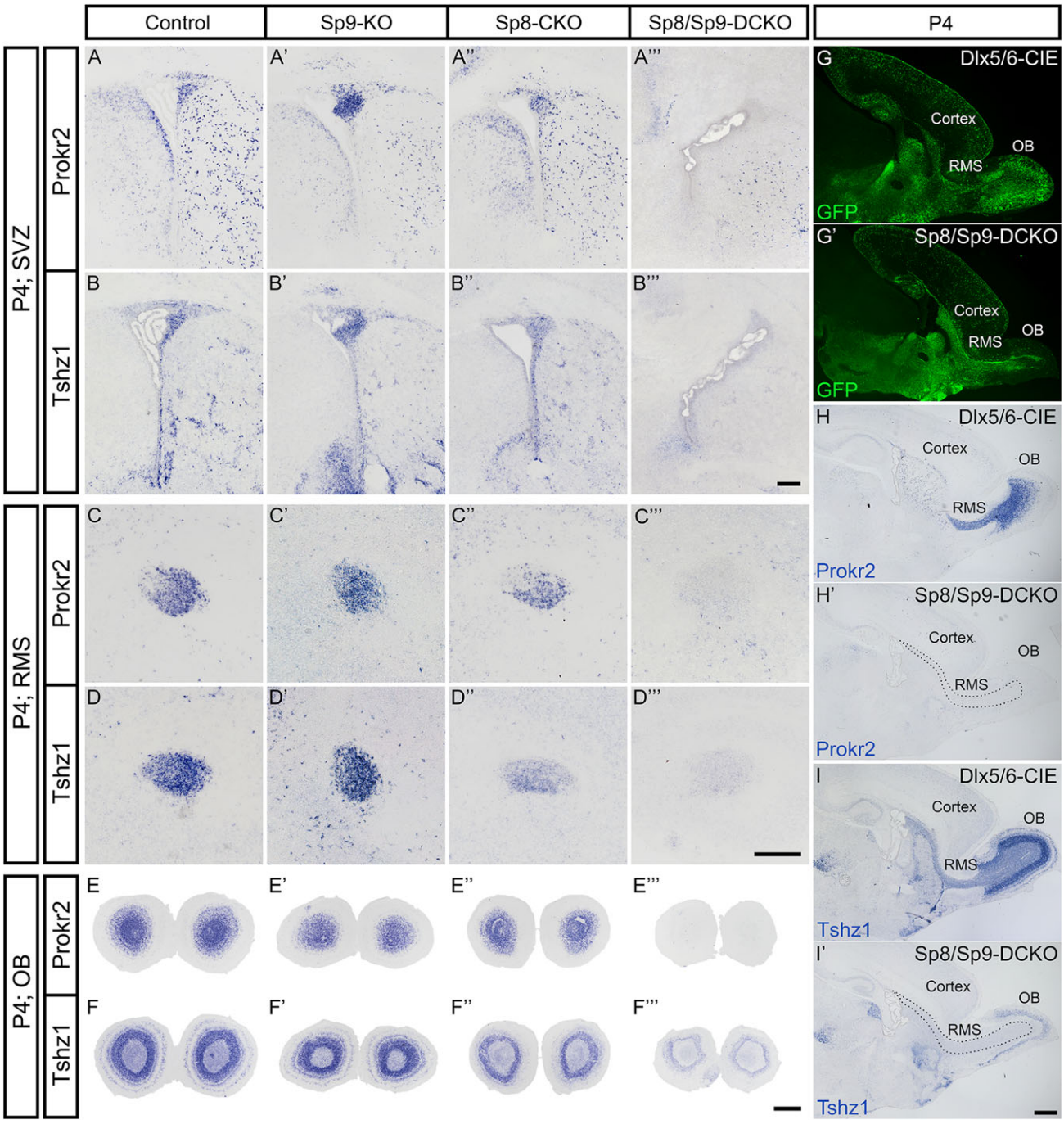

Figure 8. *Prokr2* and *Tshz1* expression in the postnatal V-SVZ, RMS, and OB are dependent on Sp8 and Sp9. (*A*–*I*′) *Prokr2* and *Tshz1* expression in the V-SVZ, RMS, and OB were observed in coronal (*A*–*F*‴) and sagittal (*G*–*I*′) sections of control, *Sp9-KO*, *Sp8-CKO* mice at P4, whereas their expression were lost from these structures in *Sp8/Sp9-DCKO* mice. Note remaining *Tshz1* expression in mitral/tufted cells in the *Sp8/Sp9-DCKO* OB (*F*‴, *I*′). Scale bars: 200 μm in *B*‴ for *A*–*B*‴; 200 μm in *D*‴ for *C*–*D*‴; 500 μm in *F*‴ for *E*–*F*‴; 500 μm in *I*′ for *G*–*I*′.

Taken together, our RNA-Seq and in situ hybridization analysis showed that the expressions of *Tshz1* and *Prokr2* in the embryonic dLGE and in the postnatal V-SVZ–RMS–OB critically depend on Sp8 and Sp9 function (Supplementary Fig. S6).

Discussion

Our results indicate that the transcription programs regulated by *Sp8* and *Sp9* are essential for OB interneuron differentiation, tangential and radial migration, and cell survival (Supplementary Fig. S6). This regulation is mainly due to promoting *Prokr2* and *Tshz1* expression by Sp8 and Sp9, as in *Sp8/Sp9-DCKO*, neuroblasts in the V-SVZ–RMS–OB system fail to express *Prokr2* and *Tshz1*. Furthermore, *Sp8/Sp9-DCKO* mice largely phenocopy *Prokr2* and *Tshz1* mutants in the V-SVZ–RMS–OB system and vice versa. This study may provide novel insights into the mechanisms underlying Kallmann syndrome.

Sp8 and *Sp9* are Important for Lineage Progression From Neural Progenitors to OB interneurons

OB neurogenesis in rodents is a continuous process of neuron production from neural stem/progenitor cells throughout embryonic development and adulthood. A previous study has shown that *miR-124* regulates the temporal progression of neurogenesis in the adult V-SVZ (Cheng et al. 2009). Here we propose that *Sp8* and *Sp9* also regulate the lineage progression of neural stem/progenitor cells in the V-SVZ and RMS (Supplementary Fig. S6). This is based on several observations:

1. Sp8 and Sp9 are expressed in a small fraction of Ascl1$^+$ progenitors (Waclaw et al. 2006; Zhang et al. 2016), and are continuously expressed by dividing neuroblasts, postmitotic neuroblasts, immature and mature OB interneurons, indicating that they may control some or all steps in this neurogenic process.
2. Conditional inactivation of *Sp8* and *Sp9* results in accumulation of Gsx2$^+$ and Ascl1$^+$ progenitors and dividing DCX$^+$ neuroblasts in the V-SVZ and OB, and a severe reduction in OB interneurons. Especially, although many more Gsx2$^+$, Ascl1$^+$, BrdU$^+$, and BrdU$^+$/DCX$^+$ cells were observed in the adult *hGFAP-Cre*; *Sp8*$^{F/F}$; *Sp9*$^{F/F}$ mouse OBs, there were a ~3-fold decrease of *DCX* expression compared with controls (Supplementary Fig. S2, Supplementary Table S3), strongly suggesting blockage of neuronal differentiation in these progenitors.
3. *Sp8* expression in neuroblasts in the dLGE and the postnatal V-SVZ, RMS, and OB depends on the *Dlx1* and *Dlx2* transcription factors. *Dlx1* and *Dlx2* are key regulators of interneuron genesis. They are expressed in neural progenitors as well as in migratory neuroblasts in the V-SVZ–RMS–OB system (Porteus et al. 1994; Anderson et al. 1997; Doetsch et al. 2002; Lim et al. 2006, 2009; Long et al. 2007, 2009). In *Dlx1* and *Dlx2* double mutants, *Sp8* expression is completely lost in these neurogenic regions (Long et al. 2007, 2009).
4. The homeodomain transcription factor Gsx2 is at the top hierarchy of LGE identity, and induces *Ascl1* and *Dlx2* expression in the LGE (Corbin et al. 2000; Toresson et al. 2000; Yun et al. 2001; Waclaw et al. 2009; Wang et al. 2013). In the adult V-SVZ, *Gsx2* is expressed in a subset of neural stem/progenitor cells and promotes the activation and lineage progression of neural stem cells (Lopez-Juarez et al. 2013). *Sp8* expression in the dLGE, adult V-SVZ and OB depends on *Gsx2* (Waclaw et al. 2006; Lopez-Juarez et al. 2013) and *Gsx2*$^+$ neural progenitor differentiation is blocked in the V-SVZ–RMS–OB system of *Sp8/Sp9-DCKO* mice.
5. The downstream targets of Sp8 and Sp9 are *Prokr2* and *Tshz1*, as newly born neuroblasts fail to express *Prokr2* and *Tshz1* in the absence of Sp8/9 function. Note that *Prokr2* and *Tshz1* are required to promote neuronal differentiation and migration in the V-SVZ–RMS–OB (Ng et al. 2005; Matsumoto et al. 2006; Prosser et al. 2007; Ragancokova et al. 2014).

Cell Death in the V-SVZ–RMS–OB in the Absence of *Sp8* and *Sp9*

Increased apoptotic cell death also contributed to the defects in the *Sp8/Sp9-DCKO* in the V-SVZ, RMS, and OB. *Sp8* and *Sp9* may be directly required for the survival of these cells. However, we cannot exclude that some of the effect on cell survival may be indirect or cell nonautonomous. The *Sp8-CKO* mice also showed increased apoptosis within the dLGE at late embryonic stages as well as in the postnatal RMS and OB (Waclaw et al. 2006). We have found that Sp9 promotes the survival of postmitotic striatopallidal projection neurons (Zhang et al. 2016).

Redundant Functions of *Sp8* and *Sp9* in Regulating OB Interneuron Development

During development, *Sp8* is expressed in the cortical VZ and regulates cortical patterning (Sahara et al. 2007; Zembrzycki et al. 2007; Borello et al. 2014), whereas *Sp9* is required for making most Drd2 striatopallidal medium-sized spiny neurons (Zhang et al. 2016). *Sp8* also plays a role in establishing the pMN/p3 domain boundary in the spinal cord (Li et al. 2014). Therefore, *Sp8* and *Sp9* each has prominent unique functions that are related at least in part due to differences in their expression patterns. For the development of OB interneurons, *Sp8*'s function (Waclaw et al. 2006; Li et al. 2011) appears more prominent than *Sp9*, as we did not observe major OB interneuron defect in *Sp9* single mutants (Fig. 1*F–J*), and upregulation of *Sp8* expression is likely to compensate for the loss of *Sp9* in the OB of *Sp9-KO* mice (Supplementary Fig. S1*M*, *N*).

In this study, we found redundant role for *Sp8* and *Sp9* in promoting *Prokr2* and *Tshz1* expression. This was evident in virtually all neuroblasts in the embryonic dLGE and in the postnatal V-SVZ, RMS, and OB, suggesting that rules governing OB interneuron genesis from embryonic to adult stages are maintained. While the defects of tangential and radial migration of neuroblasts in the *Sp8* and *Sp9* single mutant OB were not apparent (mainly because *Prokr2* and *Tshz1* expressions were largely unaffected), we demonstrate that *Sp8* and *Sp9* coordinately promote the tangential and radial migration of neuroblasts in the V-SVZ–RMS–OB system in a cell-autonomous manner. A similar function has been proposed for *Prok2-Prokr2* signaling (Ng et al. 2005; Matsumoto et al. 2006; Prosser et al. 2007) and/or *Tshz1* (Ragancokova et al. 2014). *Sp8* and *Sp9* may also coordinately promote *Meis1*, *Vax1*, and *Pbx3* expression in the V-SVZ–RMS–OB (Supplementary Fig. S4*G–L′*, Supplementary Table S1), 3 additional transcription factors important for OB development (Soria et al. 2004). Within the zinc-finger domain (DNA binding domain), only one amino acid residue differs between Sp8 and Sp9 (Kawakami et al. 2004; Zhao and Meng 2005). Therefore, Sp8 and Sp9 are likely to directly bind to the same set of target genes (e.g., promoters and enhancers). The redundancy of *Sp8* and *Sp9* may ensure normal OB interneuron development. Clearly the deletion of these 2 transcription factors has a broad impact on OB development and particularly on the generation and migration of interneurons, a process that is continuous throughout life in rodents.

A recent study suggests that Tshz1 directly binds to a regulatory element of *Prokr2* to promote its expression in neuroblasts that are migrating radially within the OB (Ragancokova et al. 2014). However, it is worth noting that *Prokr2* expression in neuroblasts in the V-SVZ and RMS does not depend on Tshz1 (Ragancokova et al. 2014). In addition, *Tshz1* expression in mature OB interneurons does not correlate with *Prokr2* expression (Ragancokova et al. 2014) (Supplementary Fig. S5*B′*, *C′*, this study).

Sp8/Sp9 and Kallmann Syndrome

Kallmann syndrome has 2 main clinical manifestations: congenital hypogonadotropic hypogonadism and anosmia/hyposmia. Both *PROK2* and *PROKR2* mutations are implicated in Kallmann syndrome (Dode et al. 2006; Sarfati et al. 2010; Martin et al. 2011),

and both *Prok2* and *Prokr2* mutant mice recapitulate the human Kallmann syndrome phenotype, including hypogonadotropic hypogonadism caused by GnRH deficiency (Ng et al. 2005; Matsumoto et al. 2006; Pitteloud et al. 2007; Prosser et al. 2007). *Sp8* and *Sp9* are widely expressed in the human dLGE and infant V-SVZ, RMS, and OB (Ma et al. 2013; Wang et al. 2014) (data not shown). Herein, we found that *Sp8* and *Sp9* coordinately promote the expression of *Prokr2* and *Tshz1* in the migratory neuroblasts, whereas *Prokr2* and *Tshz1* expression in *Sp8* and *Sp9* single mutants were largely unaffected. These results suggest that *Sp8* and *Sp9* directly regulate OB interneuron development through inducing the expression of molecules involved in human Kallmann syndrome. Future studies are needed to determine whether loss of *Sp8* and *Sp9* also contribute to other aspects of Kallmann syndrome, such as the generation and migration of GnRH neurons.

Author Contributions

J.L. and C.W. performed all experiments and analysis. Z.Z., Y. W., L.A., Q.L., Z.X., S.W., W.L., T.G., G.L., G.T., Y.Y., H.D. and Z.F. helped conduct experiments and analyze the data. M.H., B.C., K.C. A.A.-B. and J.L.R. helped guide the project and analyzed some results. Z.Y. designed the experiments, analyzed the results and wrote the article.

Supplementary Material

Supplementary data are available at Cerebral Cortex online.

Funding

Research grants to Z.Y. from National Natural Science Foundation of China (31425011, 31630032, 31421091, and 31429002), research grants to B.C. from NIH (NS089777), K.C. from NIH (MH090740 and NS044080), and J.L. Rubenstein from NIH (MH049428).

Notes

The GEO accession number for the RNA-Seq data reported in this article is GSE87417. *Conflict of Interest*: J.L.R. and A.A.B. are cofounders, stockholders, and currently serve on the scientific board of Neurona, a company studying the potential therapeutic use of interneuron transplantation.

References

Alonso M, Ortega-Perez I, Grubb MS, Bourgeois JP, Charneau P, Lledo PM. 2008. Turning astrocytes from the rostral migratory stream into neurons: a role for the olfactory sensory organ. J Neurosci. 28:11089–11102.

Andersen J, Urban N, Achimastou A, Ito A, Simic M, Ullom K, Martynoga B, Lebel M, Goritz C, Frisen J, et al. 2014. A transcriptional mechanism integrating inputs from extracellular signals to activate hippocampal stem cells. Neuron. 83: 1085–1097.

Anderson SA, Qiu M, Bulfone A, Eisenstat DD, Meneses J, Pedersen R, Rubenstein JL. 1997. Mutations of the homeobox genes Dlx-1 and Dlx-2 disrupt the striatal subventricular zone and differentiation of late born striatal neurons. Neuron. 19:27–37.

Bartolini G, Ciceri G, Marin O. 2013. Integration of GABAergic interneurons into cortical cell assemblies: lessons from embryos and adults. Neuron. 79:849–864.

Bell SM, Schreiner CM, Waclaw RR, Campbell K, Potter SS, Scott WJ. 2003. Sp8 is crucial for limb outgrowth and neuropore closure. Proc Natl Acad Sci USA. 100:12195–12200.

Bertrand N, Castro DS, Guillemot F. 2002. Proneural genes and the specification of neural cell types. Nat Rev Neurosci. 3: 517–530.

Borello U, Madhavan M, Vilinsky I, Faedo A, Pierani A, Rubenstein J, Campbell K. 2014. Sp8 and COUP-TF1 reciprocally regulate patterning and Fgf signaling in cortical progenitors. Cereb Cortex. 24:1409–1421.

Carleton A, Petreanu LT, Lansford R, Alvarez-Buylla A, Lledo PM. 2003. Becoming a new neuron in the adult olfactory bulb. Nat Neurosci. 6:507–518.

Castro DS, Martynoga B, Parras C, Ramesh V, Pacary E, Johnston C, Drechsel D, Lebel-Potter M, Garcia LG, Hunt C, et al. 2011. A novel function of the proneural factor Ascl1 in progenitor proliferation identified by genome-wide characterization of its targets. Genes Dev. 25:930–945.

Cheng LC, Pastrana E, Tavazoie M, Doetsch F. 2009. miR-124 regulates adult neurogenesis in the subventricular zone stem cell niche. Nat Neurosci. 12:399–408.

Corbin JG, Gaiano N, Machold RP, Langston A, Fishell G. 2000. The Gsh2 homeodomain gene controls multiple aspects of telencephalic development. Development. 127:5007–5020.

Dode C, Teixeira L, Levilliers J, Fouveaut C, Bouchard P, Kottler ML, Lespinasse J, Lienhardt-Roussie A, Mathieu M, Moerman A, et al. 2006. Kallmann syndrome: mutations in the genes encoding prokineticin-2 and prokineticin receptor-2. PLoS Genet. 2: e175.

Doetsch F, Alvarez-Buylla A. 1996. Network of tangential pathways for neuronal migration in adult mammalian brain. Proc Natl Acad Sci U S A. 93:14895–14900.

Doetsch F, Caille I, Lim DA, Garcia-Verdugo JM, Alvarez-Buylla A. 1999. Subventricular zone astrocytes are neural stem cells in the adult mammalian brain. Cell. 97:703–716.

Doetsch F, Garcia-Verdugo JM, Alvarez-Buylla A. 1997. Cellular composition and three-dimensional organization of the subventricular germinal zone in the adult mammalian brain. J Neurosci. 17:5046–5061.

Doetsch F, Petreanu L, Caille I, Garcia-Verdugo JM, Alvarez-Buylla A. 2002. EGF converts transit-amplifying neurogenic precursors in the adult brain into multipotent stem cells. Neuron. 36:1021–1034.

Hack I, Bancila M, Loulier K, Carroll P, Cremer H. 2002. Reelin is a detachment signal in tangential chain-migration during postnatal neurogenesis. Nat Neurosci. 5:939–945.

Imayoshi I, Kageyama R. 2014. bHLH factors in self-renewal, multipotency, and fate choice of neural progenitor cells. Neuron. 82:9–23.

Kawakami Y, Esteban CR, Matsui T, Rodriguez-Leon J, Kato S, Izpisua Belmonte JC. 2004. Sp8 and Sp9, two closely related buttonhead-like transcription factors, regulate Fgf8 expression and limb outgrowth in vertebrate embryos. Development. 131:4763–4774.

Kawasawa YI, Salzberg AC, Li M, Sestan N, Greer CA, Imamura F. 2016. RNA-seq analysis of developing olfactory bulb projection neurons. Mol Cell Neurosci. 74:78–86.

Kohwi M, Petryniak MA, Long JE, Ekker M, Obata K, Yanagawa Y, Rubenstein JL, Alvarez-Buylla A. 2007. A subpopulation of olfactory bulb GABAergic interneurons is derived from Emx1- and Dlx5/6-expressing progenitors. J Neurosci. 27:6878–6891.

Kosaka T, Kosaka K. 2012. Further characterization of the juxtaglomerular neurons in the mouse main olfactory bulb by transcription factors, Sp8 and Tbx21. Neurosci Res. 73:24–31.

Li X, Liu Z, Qiu M, Yang Z. 2014. Sp8 plays a supplementary role to Pax6 in establishing the pMN/p3 domain boundary in the spinal cord. Development. 141:2875–2884.

Li X, Sun C, Lin C, Ma T, Madhavan MC, Campbell K, Yang Z. 2011. The transcription factor Sp8 is required for the production of parvalbumin-expressing interneurons in the olfactory bulb. J Neurosci. 31:8450–8455.

Lim DA, Alvarez-Buylla A. 2016. The adult ventricular-subventricular zone (V-SVZ) and olfactory bulb (OB) neurogenesis. Cold Spring Harb Perspect Biol. 8: pii: a018820. doi: 10.1101/cshperspect.a018820.

Lim DA, Huang YC, Swigut T, Mirick AL, Garcia-Verdugo JM, Wysocka J, Ernst P, Alvarez-Buylla A. 2009. Chromatin remodelling factor Mll1 is essential for neurogenesis from postnatal neural stem cells. Nature. 458:529–533.

Lim DA, Suarez-Farinas M, Naef F, Hacker CR, Menn B, Takebayashi H, Magnasco M, Patil N, Alvarez-Buylla A. 2006. In vivo transcriptional profile analysis reveals RNA splicing and chromatin remodeling as prominent processes for adult neurogenesis. Mol Cell Neurosci. 31:131–148.

Liu F, You Y, Li X, Ma T, Nie Y, Wei B, Li T, Lin H, Yang Z. 2009. Brain injury does not alter the intrinsic differentiation potential of adult neuroblasts. J Neurosci. 29:5075–5087.

Lois C, Alvarez-Buylla A. 1994. Long-distance neuronal migration in the adult mammalian brain. Science. 264:1145–1148.

Lois C, Garcia-Verdugo JM, Alvarez-Buylla A. 1996. Chain migration of neuronal precursors. Science. 271:978–981.

Long JE, Garel S, Alvarez-Dolado M, Yoshikawa K, Osumi N, Alvarez-Buylla A, Rubenstein JL. 2007. Dlx-dependent and -independent regulation of olfactory bulb interneuron differentiation. J Neurosci. 27:3230–3243.

Long JE, Swan C, Liang WS, Cobos I, Potter GB, Rubenstein JL. 2009. Dlx1&2 and Mash1 transcription factors control striatal patterning and differentiation through parallel and overlapping pathways. J Comp Neurol. 512:556–572.

Lopez-Juarez A, Howard J, Ullom K, Howard L, Grande A, Pardo A, Waclaw R, Sun YY, Yang D, Kuan CY, et al. 2013. Gsx2 controls region-specific activation of neural stem cells and injury-induced neurogenesis in the adult subventricular zone. Genes Dev. 27:1272–1287.

Ma T, Wang C, Wang L, Zhou X, Tian M, Zhang Q, Zhang Y, Li J, Liu Z, Cai Y, et al. 2013. Subcortical origins of human and monkey neocortical interneurons. Nat Neurosci. 16: 1588–1597.

Malatesta P, Hack MA, Hartfuss E, Kettenmann H, Klinkert W, Kirchhoff F, Gotz M. 2003. Neuronal or glial progeny: regional differences in radial glia fate. Neuron. 37:751–764.

Martin C, Balasubramanian R, Dwyer AA, Au MG, Sidis Y, Kaiser UB, Seminara SB, Pitteloud N, Zhou QY, Crowley WFJr. 2011. The role of the prokineticin 2 pathway in human reproduction: evidence from the study of human and murine gene mutations. Endocr Rev. 32:225–246.

Matsumoto S, Yamazaki C, Masumoto KH, Nagano M, Naito M, Soga T, Hiyama H, Matsumoto M, Takasaki J, Kamohara M, et al. 2006. Abnormal development of the olfactory bulb and reproductive system in mice lacking prokineticin receptor PKR2. Proc Natl Acad Sci U S A. 103:4140–4145.

Merkle FT, Fuentealba LC, Sanders TA, Magno L, Kessaris N, Alvarez-Buylla A. 2014. Adult neural stem cells in distinct microdomains generate previously unknown interneuron types. Nat Neurosci. 17:207–214.

Merkle FT, Mirzadeh Z, Alvarez-Buylla A. 2007. Mosaic organization of neural stem cells in the adult brain. Science. 317: 381–384.

Mirzadeh Z, Doetsch F, Sawamoto K, Wichterle H, Alvarez-Buylla A. 2010. The subventricular zone en-face: whole-mount staining and ependymal flow. J Vis Exp. 39: pii: 1938. doi: 10.3791/1938.

Mirzadeh Z, Merkle FT, Soriano-Navarro M, Garcia-Verdugo JM, Alvarez-Buylla A. 2008. Neural stem cells confer unique pinwheel architecture to the ventricular surface in neurogenic regions of the adult brain. Cell Stem Cell. 3:265–278.

Nagayama S, Homma R, Imamura F. 2014. Neuronal organization of olfactory bulb circuits. Front Neural Circuits. 8:98.

Ng KL, Li JD, Cheng MY, Leslie FM, Lee AG, Zhou QY. 2005. Dependence of olfactory bulb neurogenesis on prokineticin 2 signaling. Science. 308:1923–1927.

Pei Z, Wang B, Chen G, Nagao M, Nakafuku M, Campbell K. 2011. Homeobox genes Gsx1 and Gsx2 differentially regulate telencephalic progenitor maturation. Proc Natl Acad Sci U S A. 108:1675–1680.

Petreanu L, Alvarez-Buylla A. 2002. Maturation and death of adult-born olfactory bulb granule neurons: role of olfaction. J Neurosci. 22:6106–6113.

Pitteloud N, Zhang C, Pignatelli D, Li JD, Raivio T, Cole LW, Plummer L, Jacobson-Dickman EE, Mellon PL, Zhou QY, et al. 2007. Loss-of-function mutation in the prokineticin 2 gene causes Kallmann syndrome and normosmic idiopathic hypogonadotropic hypogonadism. Proc Natl Acad Sci U S A. 104:17447–17452.

Ponti G, Obernier K, Guinto C, Jose L, Bonfanti L, Alvarez-Buylla A. 2013. Cell cycle and lineage progression of neural progenitors in the ventricular-subventricular zones of adult mice. Proc Natl Acad Sci U S A. 110:E1045–E1054.

Porteus MH, Bulfone A, Liu JK, Puelles L, Lo LC, Rubenstein JL. 1994. DLX-2, MASH-1, and MAP-2 expression and bromodeoxyuridine incorporation define molecularly distinct cell populations in the embryonic mouse forebrain. J Neurosci. 14:6370–6383.

Prosser HM, Bradley A, Caldwell MA. 2007. Olfactory bulb hypoplasia in Prokr2 null mice stems from defective neuronal progenitor migration and differentiation. Eur J Neurosci. 26: 3339–3344.

Ragancokova D, Rocca E, Oonk AM, Schulz H, Rohde E, Bednarsch J, Feenstra I, Pennings RJ, Wende H, Garratt AN. 2014. TSHZ1-dependent gene regulation is essential for olfactory bulb development and olfaction. J Clin Invest. 124:1214–1227.

Saghatelyan A, de Chevigny A, Schachner M, Lledo PM. 2004. Tenascin-R mediates activity-dependent recruitment of neuroblasts in the adult mouse forebrain. Nat Neurosci. 7: 347–356.

Sahara S, Kawakami Y, Izpisua Belmonte JC, O'Leary DD. 2007. Sp8 exhibits reciprocal induction with Fgf8 but has an opposing effect on anterior-posterior cortical area patterning. Neural Dev. 2:10.

Sarfati J, Dode C, Young J. 2010. Kallmann syndrome caused by mutations in the PROK2 and PROKR2 genes: pathophysiology and genotype-phenotype correlations. Front Horm Res. 39:121–132.

Sawamoto K, Wichterle H, Gonzalez-Perez O, Cholfin JA, Yamada M, Spassky N, Murcia NS, Garcia-Verdugo JM, Marin O, Rubenstein JL, et al. 2006. New neurons follow the flow of cerebrospinal fluid in the adult brain. Science. 311:629–632.

Shepherd GM, Chen WR, Willhite D, Migliore M, Greer CA. 2007. The olfactory granule cell: from classical enigma to central role in olfactory processing. Brain Res Rev. 55:373–382.

Soria JM, Taglialatela P, Gil-Perotin S, Galli R, Gritti A, Verdugo JM, Bertuzzi S. 2004. Defective postnatal neurogenesis and

disorganization of the rostral migratory stream in absence of the Vax1 homeobox gene. J Neurosci. 24:11171–11181.

Srinivas S, Watanabe T, Lin CS, William CM, Tanabe Y, Jessell TM, Costantini F. 2001. Cre reporter strains produced by targeted insertion of EYFP and ECFP into the ROSA26 locus. BMC Dev Biol. 1:4.

Stenman J, Toresson H, Campbell K. 2003. Identification of two distinct progenitor populations in the lateral ganglionic eminence: implications for striatal and olfactory bulb neurogenesis. J Neurosci. 23:167–174.

Toresson H, Potter SS, Campbell K. 2000. Genetic control of dorsal-ventral identity in the telencephalon: opposing roles for Pax6 and Gsh2. Development. 127:4361–4371.

Trapnell C, Roberts A, Goff L, Pertea G, Kim D, Kelley DR, Pimentel H, Salzberg SL, Rinn JL, Pachter L. 2012. Differential gene and transcript expression analysis of RNA-seq experiments with TopHat and Cufflinks. Nat Protoc. 7:562–578.

Tucker ES, Polleux F, LaMantia AS. 2006. Position and time specify the migration of a pioneering population of olfactory bulb interneurons. Dev Biol. 297:387–401.

Vergano-Vera E, Yusta-Boyo MJ, de Castro F, Bernad A, de Pablo F, Vicario-Abejon C. 2006. Generation of GABAergic and dopaminergic interneurons from endogenous embryonic olfactory bulb precursor cells. Development. 133:4367–4379.

Waclaw RR, Allen ZJ2nd, Bell SM, Erdelyi F, Szabo G, Potter SS, Campbell K. 2006. The zinc finger transcription factor Sp8 regulates the generation and diversity of olfactory bulb interneurons. Neuron. 49:503–516.

Waclaw RR, Wang B, Pei Z, Ehrman LA, Campbell K. 2009. Distinct temporal requirements for the homeobox gene Gsx2 in specifying striatal and olfactory bulb neuronal fates. Neuron. 63:451–465.

Wang B, Long JE, Flandin P, Pla R, Waclaw RR, Campbell K, Rubenstein JL. 2013. Loss of Gsx1 and Gsx2 function rescues distinct phenotypes in Dlx1/2 mutants. J Comp Neurol. 521: 1561–1584.

Wang B, Lufkin T, Rubenstein JL. 2011. Dlx6 regulates molecular properties of the striatum and central nucleus of the amygdala. J Comp Neurol. 519:2320–2334.

Wang C, You Y, Qi D, Zhou X, Wang L, Wei S, Zhang Z, Huang W, Liu Z, Liu F, et al. 2014. Human and monkey striatal interneurons are derived from the medial ganglionic eminence but not from the adult subventricular zone. J Neurosci. 34:10906–10923.

Wei B, Nie Y, Li X, Wang C, Ma T, Huang Z, Tian M, Sun C, Cai Y, You Y, et al. 2011. Emx1-expressing neural stem cells in the subventricular zone give rise to new interneurons in the ischemic injured striatum. Eur J Neurosci. 33:819–830.

Wichterle H, Turnbull DH, Nery S, Fishell G, Alvarez-Buylla A. 2001. In utero fate mapping reveals distinct migratory pathways and fates of neurons born in the mammalian basal forebrain. Development. 128:3759–3771.

Young KM, Fogarty M, Kessaris N, Richardson WD. 2007. Subventricular zone stem cells are heterogeneous with respect to their embryonic origins and neurogenic fates in the adult olfactory bulb. J Neurosci. 27:8286–8296.

Yun K, Potter S, Rubenstein JL. 2001. Gsh2 and Pax6 play complementary roles in dorsoventral patterning of the mammalian telencephalon. Development. 128:193–205.

Zembrzycki A, Griesel G, Stoykova A, Mansouri A. 2007. Genetic interplay between the transcription factors Sp8 and Emx2 in the patterning of the forebrain. Neural Dev. 2:8.

Zerucha T, Stuhmer T, Hatch G, Park BK, Long Q, Yu G, Gambarotta A, Schultz JR, Rubenstein JL, Ekker M. 2000. A highly conserved enhancer in the Dlx5/Dlx6 intergenic region is the site of cross-regulatory interactions between Dlx genes in the embryonic forebrain. J Neurosci. 20:709–721.

Zhang Q, Zhang Y, Wang C, Xu Z, Liang Q, An L, Li J, Liu Z, You Y, He M, et al. 2016. The zinc finger transcription factor Sp9 is required for the development of striatopallidal projection neurons. Cell Rep. 16:1431–1444.

Zhao C, Meng A. 2005. Sp1-like transcription factors are regulators of embryonic development in vertebrates. Dev Growth Differ. 47:201–211.

Zhuo L, Theis M, Alvarez-Maya I, Brenner M, Willecke K, Messing A. 2001. hGFAP-cre transgenic mice for manipulation of glial and neuronal function in vivo. Genesis. 31: 85–94.